Phases of Magmatism and Tectonics Along the Madagascar-Comoros Volcanic Chain, and Synchronous Changes in the Kinematics of the Lwandle and Somalia Plates

Anaïs Rusquet, Vincent Famin, Laurent Michon, Xavier Quidelleur, François Nauret, Martin Danišík, Gilles Ruffet, Carole Berthod, Sidonie Revillon, Patrick Bachèlery, et al.

JGR Solid Earth

RESEARCH ARTICLE
10.1029/2024JB029488

Phases of Magmatism and Tectonics Along the Madagascar-Comoros Volcanic Chain, and Synchronous Changes in the Kinematics of the Lwandle and Somalia Plates

Anaïs Rusquet[1,2], Vincent Famin[1,2], Laurent Michon[1,2], Xavier Quidelleur[3], François Nauret[4], Martin Danišík[5], Gilles Ruffet[6], Carole Berthod[1,7], Sidonie Revillon[8], Patrick Bachèlery[4], Isabelle Thinon[9], Anne Lemoine[9], Sylvie Leroy[10], Sébastien Zaragosi[11], Simon Thivet[12], Julien Bernard[9], Loraine Gourbet[13], Etienne Médard[4], and Alix Toulier[14]

[1]Université Paris Cité, Institut de Physique Du Globe de Paris, CNRS, UMR 7154, Paris, France, [2]Université de La Réunion, Laboratoire GéoSciences Réunion, Saint Denis, France, [3]Université Paris-Saclay, Laboratoire GEOPS, Orsay, France, [4]Université Clermont-Auvergne, CNRS, IRD, OPGC, Laboratoire Magmas et Volcans, Aubière, France, [5]John de Laeter Centre, Curtin University, Perth, WA, Australia, [6]Université de Rennes 1, CNRS-INSU, UMR 6118, Géosciences Rennes, Rennes, France, [7]Observatoire Volcanologique et Sismologique de La Guadeloupe, Gourbeyre, France, [8]SEDISOR/GEO-OCEAN, UMR 6538 University Brest-CNRS-IFREMER, Plouzané, France, [9]BRGM, Orléans Cédex 2, France, [10]Sorbonne Université, CNRS-INSU, Institut des Sciences de La Terre de Paris, ISTeP, Paris, France, [11]Université Bordeaux, CNRS, EPOC, EPHE, UMR 5805, Pessac, France, [12]Department of Earth Sciences, University of Geneva, Geneva, Switzerland, [13]Earth Surface Process Modelling, GFZ German Research Center for Geosciences, Potsdam, Germany, [14]Water Resources Research Center, University of Hawai'i at Mānoa, Honolulu, HI, USA

Abstract This paper aims to solve the longstanding debate on the origin of the Comoros volcanic archipelago (Mozambique Channel, Indian Ocean) concerning whether it represents a hotspot trail or a boundary between the Lwandle and Somalia plates in possible connection with the East African Rift System (EARS). To achieve this goal, we analyzed rock samples from recently discovered and previously uninvestigated volcanoes and edifices by means of geochemistry and geochronology. Major-trace element analyses and radiometric dating ($^{40}Ar/^{39}Ar$, K-Ar, and (U-Th)/He) allow us to identify a widespread phase of Comorian volcanism initiated at 9–8 Ma, involving the Zélée, Geyser, and Leven banks, three atolls east of the Comoros. Another tectono-magmatic phase initiated at 2.5 Ma led to a N-S widening of seamount volcanism, and to the progressive development of en-échelon NW-SE structures. With this new addition of atolls and seamounts, the Comoros Archipelago becomes a ~700 km-long, ~200 km-wide E-W chain extending from the Cenozoic volcanoes of Madagascar to the EARS. The reactivation of this chain at 9–8 and 2.5 Ma coincides with abrupt changes in the motion of the Somalia plate relative to the Lwandle plate, and with plate boundary modifications. The en-échelon reorganization of structures also matches the kinematic evolution of Somalia relative to Lwandle, from transtension (>3 Ma) to pure dextral slip (≤3 Ma) in the northern Mozambique Channel. We conclude that the Madagascar-Comoros volcanic chain is a branch of the EARS and a plate boundary, further strengthening the link between magmatism and the Rovuma-Lwandle-Somalia plate kinematics.

Plain Language Summary The origin of the Comoros volcanic archipelago (between East Africa and Madagascar) is a matter of a longstanding debate. Consensus is emerging that this volcanic chain, previously interpreted as due to a hotspot, might be a branch of the East African rifts, and possibly a boundary splitting the African plate into smaller blocks. We revisited the debate in the light of new volcanic rock samples recovered from fieldwork and oceanographic campaigns. Chemical analyses of rocks and their dating with natural radioactivity reveal that a widespread volcanism occurred 9–8 Ma ago, involving not only islands of the Comoros, but also three atolls east of the archipelago. A second widespread volcanism initiated 2.5 Ma ago, leading to the propagation and widening of the Comoros chain. With this new addition of seamounts and atolls, the Comoros become a ~700 km-long, ~200 km-wide E-W chain of volcanoes running from the volcanoes of Madagascar to the East African rifts. Magmatic and tectonic episodes started at 9–8 and 2.5 Ma coincide with periods of increased fragmentation of the African plate. We conclude that the Madagascar-to-Comoros volcanic chain is indeed a branch of the East African rifts and a plate boundary.

Key Points:

- Newly discovered and dated seamounts and atolls expand the Comoros Archipelago to a 700 km chain of volcanoes reaching northern Madagascar
- Two phases of magmatism and tectonic activity initiated at 9–8 and 2.5 Ma along the volcanic chain
- The phases match geometric and kinematic changes of the Lwandle and Somalia plates, confirming that the volcanic chain is a plate boundary

Supporting Information:

Supporting Information may be found in the online version of this article.

Correspondence to:

A. Rusquet,
anais.rusquet@univ-reunion.fr

Citation:

Rusquet, A., Famin, V., Michon, L., Quidelleur, X., Nauret, F., Danišík, M., et al. (2025). Phases of magmatism and tectonics along the Madagascar-Comoros Volcanic chain, and synchronous changes in the kinematics of the Lwandle and Somalia plates. *Journal of Geophysical Research: Solid Earth*, *130*, e2024JB029488. https://doi.org/10.1029/2024JB029488

Received 9 MAY 2024
Accepted 23 NOV 2024

Author Contributions:

Conceptualization: Anaïs Rusquet, Vincent Famin, Laurent Michon
Funding acquisition: Vincent Famin, Laurent Michon, Carole Berthod, Isabelle Thinon, Anne Lemoine, Sylvie Leroy, Sébastien Zaragosi
Investigation: Anaïs Rusquet, Vincent Famin, Laurent Michon, Xavier Quidelleur, François Nauret, Martin Danišík, Gilles Ruffet, Carole Berthod, Sidonie Revillon, Patrick Bachèlery, Isabelle Thinon, Anne Lemoine, Sylvie Leroy, Sébastien Zaragosi, Simon Thivet,

Julien Bernard, Loraine Gourbet, Etienne Médard, Alix Toulier
Resources: Xavier Quidelleur, Martin Danišík, Gilles Ruffet, Carole Berthod, Sidonie Revillon, Patrick Bachèlery
Writing – original draft: Anaïs Rusquet, Vincent Famin, Laurent Michon
Writing – review & editing: Xavier Quidelleur, François Nauret, Martin Danišík, Gilles Ruffet, Carole Berthod, Sidonie Revillon, Patrick Bachèlery, Isabelle Thinon, Anne Lemoine, Sylvie Leroy, Sébastien Zaragosi, Simon Thivet, Julien Bernard, Loraine Gourbet, Etienne Médard, Alix Toulier

1. Introduction

The Comoros Archipelago is a chain of volcanic islands and seamounts in the northern Mozambique Channel (Figure 1a), whose origin is the subject of a long-standing debate. This volcanic chain was first interpreted as a hotspot trail due to the apparent age progression from Mayotte in the east, presumably the oldest island, to the active volcanoes of Grande Comore Island to the west (Emerick & Duncan, 1982, 1983; Hajash & Armstrong, 1972; Figure 1b). Consequently, the Comoros Archipelago is used as a fixed reference frame for plate motion reconstructions, even though it represents an outlier in these models (Wang et al., 2018). The birth of a new submarine volcano east of Mayotte in 2018 (Cesca et al., 2020; Feuillet et al., 2021; Lemoine et al., 2020) has led to questioning of the interpretation of the Comoros as a hotspot trail and has drawn the attention of the scientific community on this poorly understood region. Alternative hypotheses are that volcanism of the Comoros is related to a crustal fracture zone (Nougier et al., 1986), and/or may even represent the northern boundary of the Lwandle plate, connecting the East African Rift System (EARS) to the volcanism and grabens of northern Madagascar (Famin et al., 2020; Michon, 2016; Michon et al., 2022; Stamps et al., 2018). Understanding the origin of the Comoros Archipelago is thus of critical importance for improving absolute plate motion reference frames, and for assessing the geodynamics of the eastern prolongation of the African rifts.

The existence of an age progression, or its absence, is of central importance in the discussion about the origin of the Comoros volcanism. Geochronological constraints have recently been revised on Anjouan and Mohéli, revealing that many ages published in the 20th century must be considered with caution (Quidelleur et al., 2022; Rusquet et al., 2023). A similar revision remains to be done for Mayotte. Moreover, recent oceanographic campaigns have unveiled a wealth of submarine volcanic structures offshore of the islands that should be included in the scheme of the Comorian volcanism, but the ages of which remain unknown (Berthod et al., 2021a; Thinon et al., 2021, 2022; Tzevahirtzian et al., 2021). Finally, the connection of the Comoros Archipelago with the Cenozoic volcanism of northern Madagascar remains unclear. A series of volcanic ridges, guyots, and atolls extends from the Comoros Archipelago eastward, yet it is not known whether these structures belong to the volcanism of the Comoros or to the Glorieuses chain of seamounts and islets extending northward. Assessing the history of subaerial and submarine volcanic structures of the northern Mozambique Channel is thus critical to improve our knowledge of the geodynamics of this region.

The objective of this study is to provide temporal and major and trace element constraints on volcanic islands and seamounts in the Comoros region, in order to compare the chronology and geochemistry of this volcanic chain with the Cenozoic volcanism of northern Madagascar, and with other geodynamic events in the western Indian Ocean. To do so, we collected subaerial samples from Mayotte to complement existing ages about the construction of this island. We also took advantage of three oceanographic cruises, PAMELA-MOZ01 (Olu, 2014), SISMAORE (Thinon et al., 2021), and SCRATCH (Berthod et al., 2021a), which mapped and dredged submarine volcanic structures in the northern Mozambique Channel. Depending on the nature and freshness of subaerial and submarine samples, we applied three radiometric dating techniques: $^{40}Ar/^{39}Ar$ on whole rock, K-Ar on groundmass, and (U-Th)/He on zircon and apatite. Combined with major and trace element analyses, these geochronological data allow us to expand the geological history of the Comorian volcanism in time toward the Miocene and in space across the northern Mozambique Channel, and to bring new arguments to the debate about the geodynamic origin of this archipelago and its connection with the volcano-tectonics of Madagascar and the EARS.

2. Geological Setting

The northern Mozambique area off East Africa is interpreted as an oblique continental margin, with the continent-ocean transition running east of the Kerimbas Graben and the Davie Fracture Zone and west of Grande Comore (Klimke et al., 2016; Mascle et al., 1987; Figure 1b). The lithosphere beneath the Comoros is thought to be oceanic (Masquelet et al., 2024; Rolandone et al., 2022), with paleo-transform faults and seafloor spreading anomalies oriented NW-SE and NE-SW, respectively (e.g., Phethean et al., 2016). With growing earthquake catalogs, it progressively becomes possible to connect the Comoros Archipelago with the other volcano-tectonic structures of the northern Mozambique Channel (Figure 1b). To the west, seismicity suggests that the Comoros alignment may be linked to the Kerimbas Graben and the Davie Fracture Zone forming part of the south-east branch of the EARS, that is, the boundary between the Rovuma block and the Lwandle and Somalia plates (Bertil et al., 2021; Michon et al., 2022). The Davie Fracture Zone and the Kerimbas Graben are devoid of

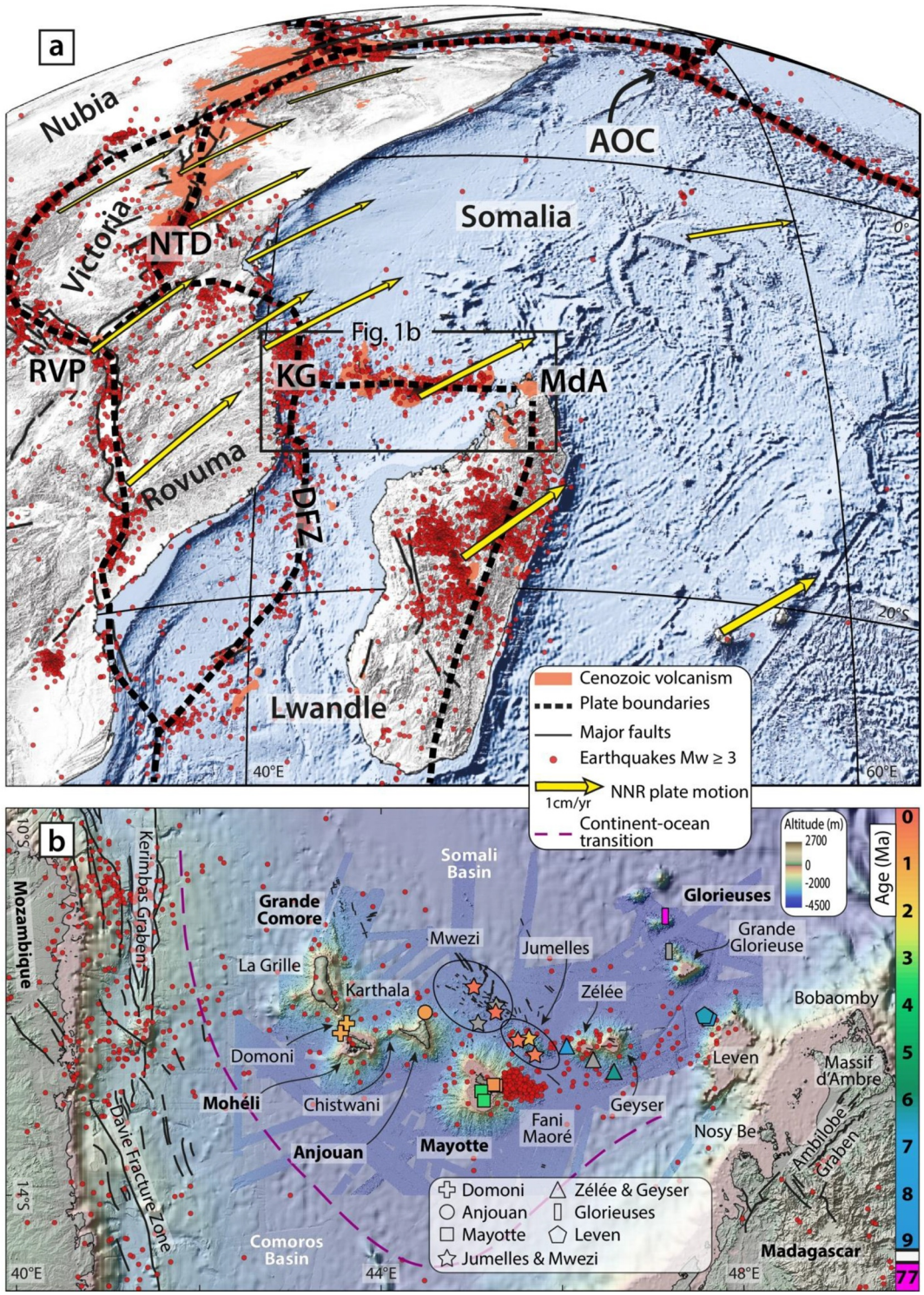

Figure 1.

Cenozoic magmatism (Franke et al., 2015), but are seismogenic structures with earthquake slip vectors consistently indicating E-W extension (e.g., Saria et al., 2014). The Kerimbas Graben initiated in the Late Miocene, and ~80% of its opening occurred since the Early Quaternary, ca. 2.5 Ma ago (Franke et al., 2015). From the Comoros Archipelago, a W-E-oriented seismicity corridor runs eastward (Figure 1a), but vanishes ~100 km before reaching the grabens of northern Madagascar (e.g., the Ambilobe Graben) and the Cenozoic volcanism of the Bobaomby Peninsula, Massif d'Ambre, and Nosy Be (Bertil et al., 2021, Figure 1b). The reason for this seismicity gap (instrumental bias or true lack of events) is unknown. The Comoros Archipelago and recently discovered submarine volcano-tectonic features in the area have been interpreted as en-échelon structures within a ~200-km-wide zone of right-lateral deformation (Famin et al., 2020; Feuillet et al., 2021; Thinon et al., 2022).

Beneath East Africa, a slow wavespeed mantle plume tail is evidenced by seismic tomography, showing that the activity of the EARS is supplied by melts from the upwelling mantle (Boyce et al., 2023). A low-velocity conduit is also found in the lower mantle beneath the Comoros (Dongmo Wamba et al., 2023). The Karthala volcano in Grande Comore shows evidence of a deep mantle plume contribution (Class et al., 1998, 2005, 2009; Class & Goldstein, 1997), whereas magmas from the other Comorian edifices (La Grille in Grande Comore, Mohéli, Anjouan, and Mayotte) are attributed to partial melting of a metasomatized, MORB-type lithospheric mantle (Bachèlery & Hémond, 2016; Bordenca et al., 2023; Pelleter et al., 2014; Späth et al., 1996). Likewise, the Cenozoic volcanism of northern Madagascar is inferred to stem from low degree partial melting of peridotite sources rich in volatiles and incompatible elements, possibly located in the lowermost lithospheric mantle (Cucciniello et al., 2011, 2016, 2022).

Grande Comore is considered to be the most recently emerged island of the archipelago, because its two volcanoes (Karthala and La Grille) are the only active subaerial eruptive vents in this region. Grande Comore Island is made of a set of N150–160°E en-échelon structures extending to the north, and a N070°E-elongated structure to the west (Thinon et al., 2022; Figure 1b). To the southeast, Grande Comore is connected to the island of Mohéli via the N155°E Domoni submarine ridge (Thinon et al., 2022; Tzevahirtzian et al., 2021). Mohéli was constructed in two stages, first as a N070°E elongated structure from >3.8 to 3 Ma, then as N110°E ridge from 2 Ma to 0.008 Ma (Rusquet et al., 2023). Drastic subsidence, during the quiescence interval between the two construction stages, from 3 to 2 Ma, drowned a carbonate platform to 400–600 m depth. Mohéli is connected to Anjouan Island via the N070°E Chistwani submarine ridge (Thinon et al., 2022; Tzevahirtzian et al., 2021), which was dated at 3.74 ± 0.05 Ma by K-Ar on groundmass (Rusquet et al., 2023; all age uncertainties are expressed hereafter at the 1σ level). On Anjouan, radiometric ages (K-Ar on groundmass and ^{14}C on charcoal) range from ~2 to 0.009 Ma (Quidelleur et al., 2022). Indents in the morphology of Anjouan indicate the occurrence of two landslides in the past 0.9 Ma of the island (Quidelleur et al., 2022).

Mayotte is thought to be the oldest island of the Comoros Archipelago. The submarine volcanism of Mayotte initiated as early as 27–26 Ma according to seismic profile interpretation (Masquelet et al., 2022). Mayotte is thought to have first emerged as two volcanoes from >10.6 to ~3 Ma, a southern edifice and a north-western edifice (Debeuf, 2004; Pelleter et al., 2014). Drowned carbonate terraces at 450–830 m depth on the southern and north-western submarine flanks of Mayotte indicate subsidence of these two volcanoes at a pace faster than the construction rate of coral reefs (Audru et al., 2006; Tzevahirtzian et al., 2021). The two volcanoes later coalesced with the construction of a third, north-eastern edifice from 2.4 Ma up to very recent (possibly Holocene) times (Lacombe et al., 2024; Zinke et al., 2003). From this north-eastern edifice, a N110°E submarine ridge runs eastward (e.g., Audru et al., 2006; Berthod et al., 2021a; Feuillet et al., 2021), at the tip of which lies the new Fani Maoré submarine volcano (Bazin et al., 2022; Lemoine et al., 2020).

Figure 1. (a) Geodynamic map of the western Indian Ocean and the East African Rift System, showing regional seismicity (NEIC catalog 1900–2022, USGS and Bertil et al., 2021), GNSS plate motion in a no net rotation (NNR, a.k.a. "absolute") reference frame (King et al., 2019), Neogene-to-present volcanism (red areas), major faults (black lines, compilations from Courgeon et al., 2018; Deville et al., 2018; Iacopini et al., 2022; Michon, 2016; Roche & Ringenbach, 2022; Roig et al., 2012), and most recent proposed plate boundaries (Michon et al., 2022; Stamps et al., 2018). AOC: Aden-Owen-Carlsberg triple junction; NTD: Northern Tanzania Divergence; RVP: Rungwe Volcanic Province; KG: Kerimbas Graben; MdA: Massif d'Ambre; DFZ: Davie Fracture Zone. (b) Sample locations in the northern Mozambique Channel. Symbol colors correspond to the color scale of radiometric ages (in Ma on the right side of the panel). Dredged samples are from the PAMELA (Olu, 2014), SISMAORE (Thinon et al., 2021), and SCRATCH (Berthod et al., 2021a) oceanographic cruises. Elevation/bathymetry grids are a compilation from bathymetric data in the northern Mozambique area (Berthod et al., 2021a; Thinon et al., 2022; Tzevahirtzian et al., 2021); 30m-gridded DEM provided by Japan Aerospace Exploration Agency (2021) and from GEBCO elsewhere (GEBCO Bathymetric Compilation Group, 2023). Also shown is the continent-ocean transition as combined from the interpretations of Mascle et al. (1987) and Klimke et al. (2016).

Northeast of Mayotte lie two N140°E submarine ridges called the Jumelles (Figure 1b). The SISMAORE cruise recently revealed that these ridges extend toward the NW as a diffuse field of volcanoes called the Mwezi province (Thinon et al., 2021, 2022). East of the Jumelles, the Zélée and Geyser banks are presumably volcanic in origin but their age is unknown. Further east of Zélée-Geyser banks, near Madagascar, lies another submarine feature called the Leven Bank (Figure 1b). This feature is possibly volcanic, according to basaltic cobbles recovered in dredges (Daniel et al., 1972). The Leven Bank lies at the junction of the Grande Comore–Mohéli–Anjouan–Mayotte–Jumelles–Zélée–Geyser E-W alignment and the NNW-SSE trend formed by the Glorieuses islets and guyots (Figure 1b). Based on radiometric dating and seismic profiles, the island of Grande Glorieuse is known to have formed by volcanism during the Cretaceous, much before the Cenozoic volcanism of the Comoros Archipelago (Leroux et al., 2020). Radiometric dating in northern Madagascar shows that igneous activity occurred since the late Oligocene to the Pleistocene from the Bobaomby Peninsula to the Massif d'Ambre, Nosy Be islands, Ampasindava Peninsula, and Tsaratanana Mountains (Cucciniello et al., 2016, and references therein). The question thus arises as whether the Leven Bank is Neogene in age and represents a link between the Comoros volcanism and the Cenozoic magmatic activity of northern Madagascar, or whether it is an older structure related to the Cretaceous magmatism of the Glorieuses trend.

3. Materials and Methods

3.1. Sampling

Submarine samples were recovered from dredging operations performed during three oceanographic campaigns, the PAMELA-MOZ01 cruise (MOZ01) onboard of the R/V *L'Atalante* (Olu, 2014), the SISMAORE cruise (SMR) on the R/V *Pourquoi Pas* (Thinon et al., 2021), and the SCRATCH cruise (SCR) on the R/V *Marion Dufresne* (Berthod et al., 2021a). Based on visual inspection, an initial sorting and selection of dredged materials was made to dispatch samples, according to their macroscopic petrology, their alteration and vesicularity, and their available quantity, for chemical and/or geochronological analyses. These samples consist of lava flows or pyroclastic breccias from different volcanic structures, including, from west to east, the Domoni Ridge (dredges MOZ01-DR07 and DR08), the northern base of Anjouan's edifice (MOZ01-DR09), the Mwezi volcanic province (SMR5 and SCR-DR03 to DR05), the two Jumelles ridges (MOZ01-DR06, SMR2, and SCR-DR07), the Zélée Bank (SMR1 and SCR-DR09), the Geyser Bank (SCR-DR10), unnamed seamounts of the Glorieuses alignment (MOZ01-DR04 and SCR-DR01), and the base of the Leven Bank (SCR-DR11 and DR12).

In addition, four onshore samples were collected on Mayotte Island to complement published radiometric ages. These subaerial samples include a phonolitic dome on southern Mayotte (19MA07), a lava flow on the west coast (18MA30), and two strombolian cones on eastern Mayotte (19MA05 and 19MA08). The location of dredges and subaerial samples is provided in Table S1.

3.2. Major-Trace Element Geochemistry

A total of 4 subaerial and 48 submarine samples were analyzed for bulk-rock major and trace elements, to classify rocks in international charts as well as to check their quality in terms of loss on ignition (LOI). Whole rock major and trace element analyses were conducted at the Pôle de Spectrométrie Océan (PSO, IUEM, Brest, France). Major element analyses follow the procedure of Cotten et al. (1995). This procedure includes the dissolution of 250 mg of rock powder in closed screw-top Savillex teflon vessels at 90°C for one day, using 3 ml of concentrated HF + 1 ml of concentrated HNO_3. Then, 96 ml of H_3BO_3 (20 g/l) in aqueous solution were added to neutralize the excess of HF. All reagents used are of analytical grade. Major elements were measured by inductively coupled plasma atomic emission spectrometry (ICP-AES, Horiba Jobin Yvon® Ultima 2 spectrometer). The boron included in the solution was used as an internal standard. Calibrations were made using the ACE, WSE, and JB2 international standards. The relative standard deviation is better than 1% for SiO_2 and 2% for other major elements.

Trace elements were measured by HR-ICP-MS (Element XR, ThermoFisher Scientific). Sample powders were weighted in PFA beakers and dissolved in a mixture of HF-HNO_3 and HCl-HNO_3 and heated on hot plates. After evaporation, residues were dissolved in 6N HCl and kept as archive solutions. An aliquot of this archive solution was taken and weighted and diluted in HNO_3 2% for analysis on the ICP-MS. Indium was added to samples as an internal standard for correcting signal drift during analysis. External standards were prepared and used for calibrating the sample concentrations. Sample analyses were interspersed with procedural blanks and geostandards

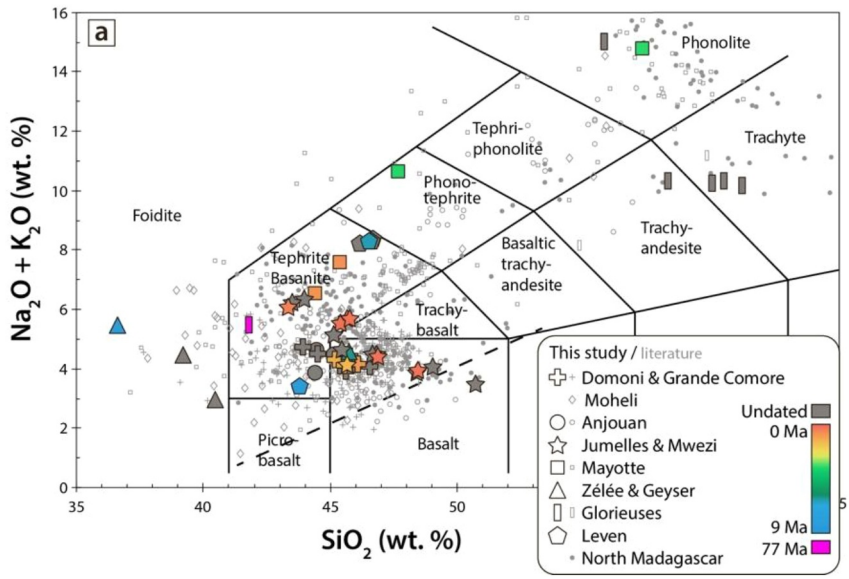

Figure 2. Major element compositions of subaerial and submarine volcanic samples from the Comoros area, Leven Bank, Glorieuses seamounts and Cenozoic North Madagascar (Bobaomby Peninsula, Massif d'Ambre, Nosy Be Archipelago) represented in a TAS diagram after normalization of the sum of oxides to 100 wt.% (Le Bas et al., 1986). The dashed line divides the alkaline and tholeiitic series (LeMaitre and International Union of Geological Sciences, 2005).

BE-N, BHVO-2, BCR-2, BIR-1, GS-N, and WS-E run as unknowns (Jochum et al., 2016). The precision obtained on the results was better than 5% for trace elements.

Our geochemical data are compared with literature major and trace elements analyses of the GEOROC database, from magmatic rocks of Anjouan (Debeuf, 2004; Flower, 1971, 1973; Nougier et al., 1986; Quidelleur et al., 2022; Thompson & Flower, 1971), Grande Comore (Class et al., 1998, 2005, 2009; Class & Goldstein, 1997; Claude-Ivanaj et al., 1998; Deniel, 1998; Desgrolard, 1996; Flower, 1971; Späth et al., 1996; Strong, 1972a; Thivet et al., 2022), Mohéli (Nougier et al., 1986; Rusquet et al., 2023; Späth et al., 1996; Strong, 1972b), Mayotte (Berthod et al., 2021b, 2021c, 2022b; Debeuf, 2004; Nougier et al., 1986; Pelleter et al., 2014; Späth et al., 1996), northern Madagascar (Bobaomby Peninsula: Cucciniello et al., 2022; Melluso et al., 2007; Nougier et al., 1986, Massif d'Ambre: Bardintzeff et al., 2010; Cucciniello et al., 2011; Nougier et al., 1986, Nosy Be Archipelago: Cucciniello et al., 2016; Melluso & Morra, 2000), and Glorieuses (Leroux et al., 2020).

3.3. Geochronology

After major and trace element analysis, 23 samples were further selected for geochronology. Three dating techniques were applied depending on the alteration of samples and their mineral phases, for allowing intermethods comparisons and avoiding the analytical bias of each technique. The $^{40}Ar/^{39}Ar$ whole rock and K-Ar groundmass techniques were applied on the freshest samples according to hand specimen inspection, thin section examination, and LOI. The (U-Th)/He dating technique on zircon and apatite was applied to samples that were too altered for the other techniques and which contained those crystals. Procedures of the three radiometric dating methods are provided in the Supporting Information S1.

4. Results

4.1. Major and Trace Elements Chemistry

Major and trace elements data are reported in Table S2 and represented in Figures 2 and 3. In a total alkali versus silica (TAS) diagram, our analyses fall in the field of alkali series, except one tholeiitic basalt from the Mwezi volcanic province (SCR-DR03; Figure 2). Samples from the Domoni Ridge (dredges MOZ01-DR07 and DR08) are basalts or basanites with SiO_2 values of 44–46.6 wt.%, and $Na_2O + K_2O$ values of 3.9–4.7 wt.%. Samples located at the base of Anjouan (MOZ01-DR09) show compositions of basalts and basanites (44.5–45.2 wt.% SiO_2

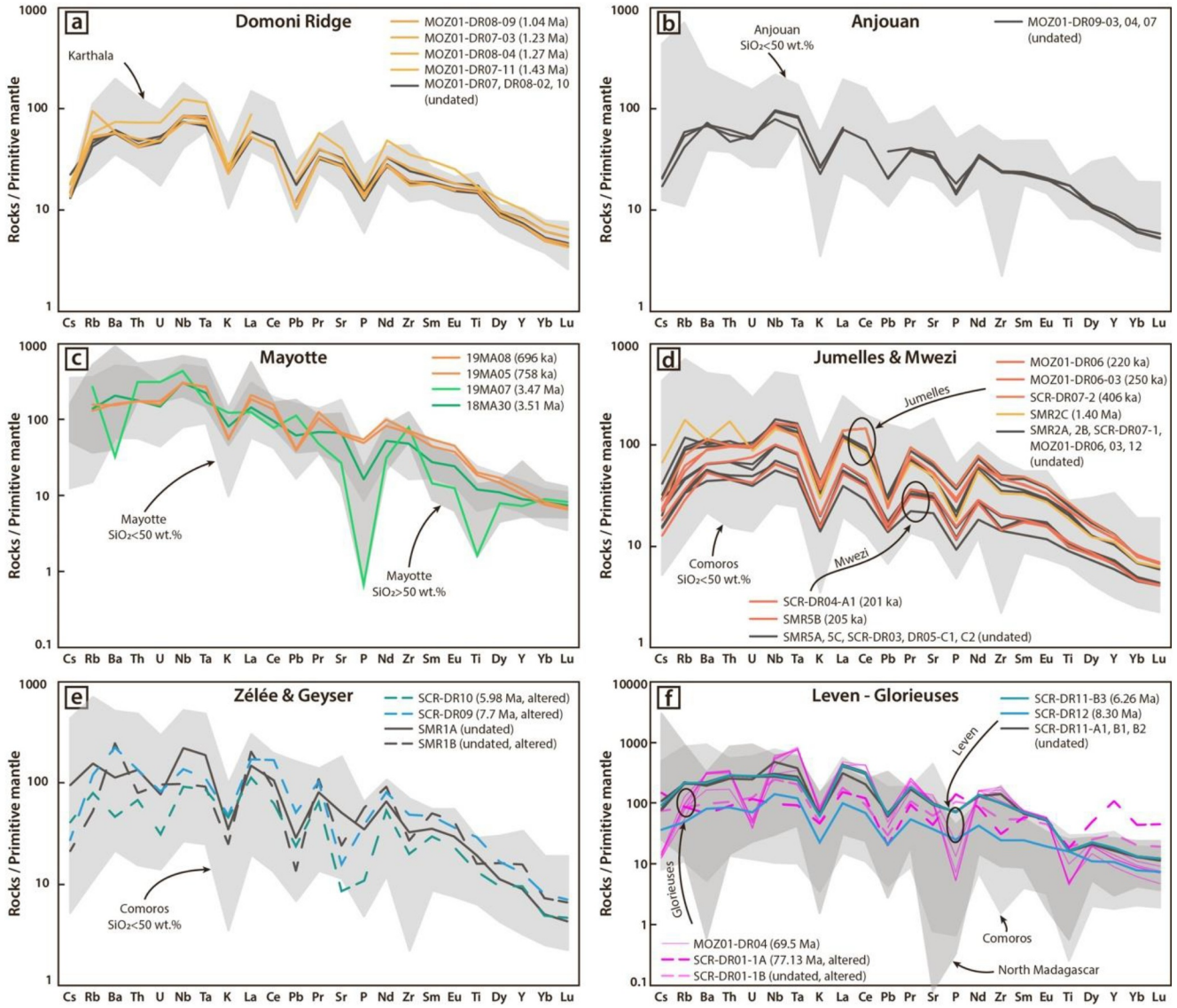

Figure 3. Spider diagrams of incompatible trace element concentrations normalized to primitive mantle values (after Lyubetskaya & Korenaga, 2007) for subaerial and submarine volcanic samples from this study. Spidergram colors follow the age chart adopted in Figures 1b and 2. Gray fields are for literature data. (a) Domoni Ridge compared to Karthala volcano in Grande Comore. (b) Anjouan offshore samples compared to subaerial data. (c) New samples compared to mafic and differentiated rocks from the literature on Mayotte. (d) Jumelles ridges and Mwezi volcanic province compared to Comorian lavas. (e) Zélée and Geyser banks compared to Comorian lavas. (f) Leven Bank and Glorieuses seamounts compared to literature data from the Comoros and from the Cenozoic volcanism of northern Madagascar (Bobaomby Peninsula, Massif d'Ambre, Nosy Be Archipelago).

and 3.8–4.6 wt.% $Na_2O + K_2O$). Mayotte subaerial samples plot along the tephri-basanite-phonolite differentiation trend (44.4–57.3 wt.% SiO_2, 6.5–14.8 wt.% $Na_2O + K_2O$), consistent with published chemical analyses. All the samples from the Mwezi volcanic province (SMR5 and SCR-DR03 to DR05) are basalts (46.7–50.8 wt.% SiO_2 and 3.5–4.5 wt.% $Na_2O + K_2O$). Some of the samples from the Jumelles ridges are basalts (SMR2: 45.2–45.8 wt.% SiO_2, 4.1–5.1 wt.% $Na_2O + K_2O$) whereas others are tephrites/basanites (MOZ01-DR06 and SCR-DR07: 43.4–45.8 wt.% SiO_2, 5.5–6.4 wt.% $Na_2O + K_2O$). Samples from the Zélée Bank (SMR1 and SCR-DR09) plot in the foidite field (36.6–40.5 wt.% SiO_2, 3–5.5 wt.% $Na_2O + K_2O$) whereas the sample from the Geyser Bank is a basalt (SCR-DR10: 45.7 wt.% SiO_2, 4.6 wt.% $Na_2O + K_2O$). Samples from the Leven Bank are basanites (SCR-DR11 and DR12: 43.7–46.7 wt.% SiO_2, 3.4–8.4 wt.% $Na_2O + K_2O$). One sample from the Glorieuses seamount (SCR-DR01-1A) is a tephrite (41.8 wt.% SiO_2, 5.4 wt.% $Na_2O + K_2O$, 0% normative olivine), another (SCR-DR01-1B) is a

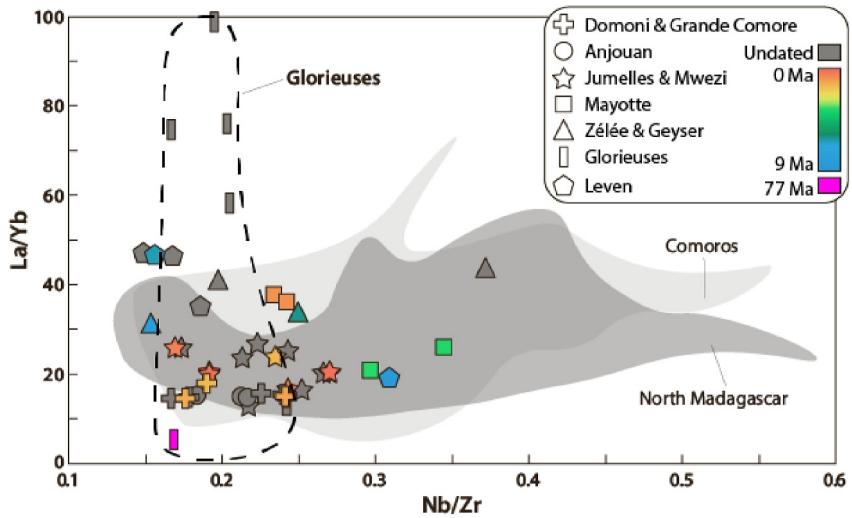

Figure 4. Nb/Zr versus La/Yb diagram of subaerial and submarine samples from the Comoros and Glorieuses, compared with the published data from the Comoros (light gray field) and Cenozoic northern Madagascar (dark gray field) already used to generate the fields in Figure 3.

phonolite (55.8. wt.% SiO_2, 15 wt.% $Na_2O + K_2O$), both with elevated LOIs (9.7–10.4 wt.%), while the rest of the samples (MOZ01-DR04-15, 16, 17, 19) fall in the trachyte field (58.29–61.20 wt.% SiO_2, 10.10–10.27 wt.% $Na_2O + K_2O$).

Several samples present elevated LOIs (up to 11.7 wt.%) as often encountered in undersaturated and differentiated melts, but also in altered rocks. Indeed, the five samples (SMR1B, SCR-DR01-1A, DR01-1B, DR09, and DR10) showing the highest LOIs (8.3–11.7 wt.%) also display textural evidence of alteration in thin sections, as indicated by the presence of secondary minerals filling voids (Figure S1 of Supporting Information S1). In the other samples, pristine olivine or feldspar crystals, fresh groundmass, and unfilled vesicles indicate an absence of significant alteration.

In spider diagrams normalized to primitive mantle, samples present marked enrichments in incompatible elements, as do all the lavas from the Comoros and Cenozoic northern Madagascar (Figure 3). Samples from the Domoni Ridge (MOZ01-DR07 and MOZ01-DR08) plot in the field of Karthala in Grande Comore (Figure 3a). Samples from submarine Anjouan plot in the field of the least differentiated rocks from subaerial Anjouan ($SiO_2 < 50$ wt.%; Figure 3b). For Mayotte (Figure 3c), our three mafic samples (18MA30, 19MA05, and 19MA08) show comparable trace element fields and patterns to literature data for the same SiO_2 range (<50 wt.%). The phonolite sample 19MA07 displays a pattern similar to published data for differentiated rocks of Mayotte ($SiO_2 > 50$ wt.%), with strong Ba, P, and Ti depletions. Samples from the Mwezi volcanic province (SMR5 and SCR-DR03 to DR05) and the Jumelles ridges (MOZ01-DR06, SMR2, and SCR-DR07) plot in the field of the least fractionated data from the Comoros (Figure 3d), with marked enrichments for the Jumelles compared to Mwezi. Samples from the Zélée and Geyser banks (SMR1, SCR-DR09 to DR10) display elevated incompatible element enrichments despite their alteration, but nevertheless plot in the fields of Comorian lavas (Figure 3e). Samples from the Leven Bank (SCR-DR11 to DR12) are in the upper range of the Comoros lavas field, except for elements such as Ce, P, and Eu, which slightly exceed the Comorian field but fit in the range of Cenozoic volcanic rocks from northern Madagascar (Figure 3f). In comparison, samples from the Glorieuses chain are above the fields of Comoros-Cenozoic northern Madagascar and Leven for either rare earth elements (REE) Dy to Lu (SCR-DR01-1A and 1B), or trace elements Ta, Ce, Pr, Nd, and Zr (other samples).

In immobile incompatible element ratios spaces such as Nb/Zr versus La/Yb, chosen for their insensitivity to alteration, samples from the Domoni Ridge, offshore Anjouan, Mayotte, the Mwezi volcanic province, the Jumelles ridges, and the Zélée-Geyser banks display values in the fields of igneous rocks from the Comoros and northern Cenozoic Madagascar (Figure 4). Some samples from the Leven Bank are in the upper range of these La/Yb values at given Nb/Zr as are some of Mayotte's published data, but nevertheless fall into these fields. On the contrary, samples from the Glorieuses chain present much more elevated La/Yb values at given Nb/Zr, and an

absence of correlation between these two ratios, plotting clearly above the Comoros and Cenozoic northern Madagascar fields.

4.2. $^{40}Ar/^{39}Ar$ Dating

$^{40}Ar/^{39}Ar$ ages and $^{37}Ar_{Ca}/^{39}Ar_K$ spectra are represented in Figure 5, and step heating data are provided in Table S3. Seven of the 10 whole rock grains analyzed allow the calculation of Pleistocene plateau ages ranging from 1.43 ± 0.07 to 0.25 ± 0.03 Ma, with relative uncertainties better than 12% of the age. The two youngest plateau ages of 0.18 ± 0.10 and 0.22 ± 0.06 Ma (samples MOZ01-DR06 and DR06-1) have larger relative uncertainties (27% and 56% of the age, respectively). One sample (MOZ01-DR08-09) gave increasing apparent ages over the whole age spectrum, which only allows the calculation of a pseudo-plateau age at 1.04 ± 0.06 Ma. Overall, samples from the Domoni Ridge are in the range 1.43 ± 0.07 to 1.23 ± 0.11 Ma ($n = 4$) or 1.43 ± 0.07 to 1.04 ± 0.06 Ma ($n = 5$) depending on whether the pseudo-plateau age is rejected or not, the uncertainties of the four other ages overlapping each other in the former case. The two dated samples from the northern base of Anjouan yielded ages of 0.95 ± 0.06 Ma and 0.94 ± 0.09 with overlapped uncertainties. The three ages of the western Jumelle ridge range from 0.25 ± 0.03 to 0.18 ± 0.10 Ma with uncertainties overlapping each other.

4.3. K-Ar Dating

New K-Ar ages on the 10 subaerial and submarine samples are reported in Table 1. Ages range from 8.297 ± 0.119 to 0.201 ± 0.010 Ma. Potassium content of the groundmass ranges from 0.683 wt.% to 5.01 wt.%, and radiogenic ^{40}Ar from 0.30% to 76.89%. For subaerial Mayotte, two ages fall in the 3.55–3.45 Ma range (18MA30, Mayotte west and 19MA07, Mount Choungi) and two others in the 0.80–0.65 Ma range (19MA05 and 19MA08, eastern Mayotte and Petite Terre). The two submarine samples from the Mwezi volcanic province, at 0.205 ± 0.016 Ma and 0.201 ± 0.010 Ma, are within uncertainty of each other. For the Jumelles ridges, one sample collected at the base of the eastern ridge falls at 1.403 ± 0.021 Ma (SMR2), whereas the other sample collected at the southern tip of the western ridge falls at 0.406 ± 0.011 Ma (SCR-DR07). For the Leven Bank, quadruplate K-Ar dating of two different groundmass density fractions (Table 1) of sample SCR-DR12 yielded overlapping uncertainties, for an average at 8.297 ± 0.119 Ma. Sample SCR-DR11-B3 falls at 6.222 ± 0.089 Ma.

4.4. (U-Th)/He Dating

The results of (U-Th)/He dating are reported in Table 2 and summarized in Figure 6. Three zircon crystals successfully extracted from submarine sample SCR-DR09 gave statistically heterogeneous ZHe dates of 332.6 ± 18.4, 205.0 ± 11.3, and 7.7 ± 0.4 Ma (Figure 6a). Apatite crystals were successfully extracted from two submarine samples, both revealing a statistically homogeneous population with an average of 6.0 ± 0.3 Ma for sample SCR-DR10 from the southern flank of the Geyser Bank (Figure 6a), and of 77.1 ± 2.3 Ma for sample SCR-DR01-1A from the dredge of an unnamed seamount north of Grande Glorieuse (Figure 6b).

5. Interpretation and Discussion

In total, four radiometric dating approaches ($^{40}Ar/^{39}Ar$ on whole rock, K-Ar on groundmass, and (U-Th)/He on zircon and apatite) were successfully applied to date 23 magmatic rocks of the northern Mozambique Channel. Adopting a closure temperature concept (Dodson, 1973), we interpret the ages obtained by these dating techniques as cooling ages, recording the timing at which the daughter isotopes cease to diffuse, which occurs at different temperatures depending on the isotopic system, the host mineral, the size of crystals and other fast diffusion pathways. For the $^{40}Ar/^{39}Ar$ system in holocrystalline whole rock and the K-Ar system in groundmass we consider the closure temperature of 200°C (e.g., McDougall & Harrison, 1999), for the (U-Th)/He system the closure temperature of 180–220°C in zircon and 60–80°C in apatite (Farley, 2002; Guenthner et al., 2013).

Our data provide chemical and temporal constraints on some of the most prominent volcano-tectonic structures that shaped the northern Mozambique Channel (Figures 7 and 8). These new constraints concern, from west to east, (a) the construction of the Domoni Ridge between the islands of Grande Comore and Mohéli, (b) the activity of northern Anjouan, (c) a reappraisal of the temporality of Mayotte's subaerial construction, (d) the construction of the Mwezi volcanic field and the Jumelles ridges, (e) the activity of the Zélée and Geyser banks, (f) the formation of the Glorieuses trend of seamounts, and (g) the volcanism of the Leven Bank.

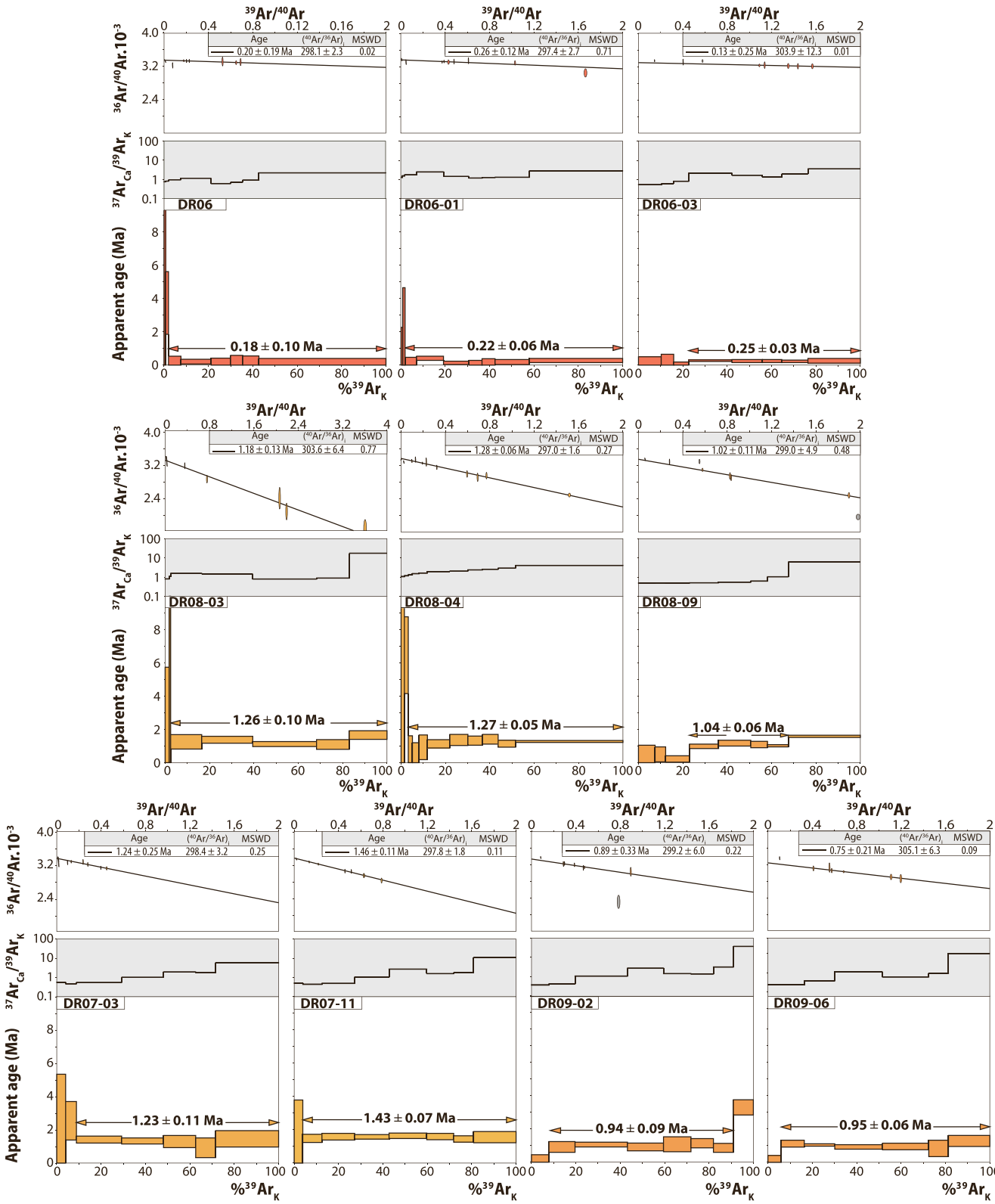

Figure 5. $^{40}Ar/^{39}Ar$ age and $^{37}Ar_{Ca}/^{39}Ar_K$ spectra of samples from dredges MOZ01-DR06, MOZ01-DR07, MOZ01-DR08 and MOZ01-DR09. Apparent age errors are 1σ and do not include errors on the J-parameter. Plateau ages are given with 1σ uncertainties including errors in the J-parameter. Inverse isochrons are represented as $^{36}Ar/^{40}Ar$ versus $^{39}Ar/^{40}Ar$ correlation diagrams, excluding gray ellipses from regression (York, 1968; York et al., 2004).

Table 1
K-Ar Dating Results of Volcanic Samples From the Northern Mozambique Channel

Sample	Province	Groundmass density interval	K (%)	^{40}Ar[a] (%)	^{40}Ar[a] (10^{11} at/g)	Age (Ma)	±1σ (Ma)	Mean age (Ma)	±1σ (Ma)	Predegassing[a]
19MA05	Mayotte	2.93–2.99	2.198	13.39	17.533	0.764	0.012	0.758	0.012	
				19.29	17.3	0.754	0.011			
19MA07	Mayotte	2.48–2.55	5.009	37.76	180.07	3.439	0.049	3.466	0.050	
				33.85	183.14	3.497	0.051			
19MA08	Mayotte	2.93–3.01	2.251	3.8	16.384	0.697	0.021	0.696	0.021	
				3.68	16.364	0.696	0.021			
18MA30	Mayotte	2.75–2.85	3.586	71.46	131.74	3.514	0.05	3.514	0.05	
				76.89	131.68	3.513	0.05			
SMR2C	Jumelles	2.95–3.02	1.327	18.8	19.387	1.398	0.021	1.403	0.021	X
				16.19	19.539	1.409	0.022			X
SCR-DR07-2	Jumelles	2.97–3.03	1.736	5.11	7.288	0.402	0.01	0.406	0.010	X
				4.43	7.4434	0.411	0.011			
SMR5B	Mwezi	2.95–3.02	0.668	1.45	1.4435	0.207	0.015	0.205	0.016	X
				1.23	1.4126	0.203	0.017			X
				0.88	1.4115	0.202	0.023			
SCR-DR04-A1	Mwezi	2.96–3.00	0.849	1.95	1.705	0.192	0.01	0.201	0.010	X
				1.93	1.7516	0.197	0.011			X
				1.27	1.9484	0.22	0.018			
SCR-DR11-B3	Leven	2.75–2.79	2.604	69.59	168.76	6.194	0.088	6.222	0.089	
				48.77	170.61	6.262	0.089			
SCR-DR12	Leven	3.00–3.06	0.683	40.68	59.798	8.359	0.12	8.345	0.119	X
				49.29	59.62	8.334	0.119			
		2.93–3.00	0.799	53.3	69.167	8.269	0.118	8.248	0.118	X
				46.45	68.786	8.224	0.118			
								8.297	0.119	

[a]Predegassing conditions are 30 min, 0.02 A.

5.1. Chronology of Volcanic Activity in the Northern Mozambique Channel

5.1.1. Domoni Ridge Construction

A first implication of our results concerns the architecture and chronology of the ridge connecting the islands of Grande Comore and Mohéli. The N155°E Domoni Ridge is aligned with the N150°E south subaerial rift zone of the active Karthala edifice in Grande Comore (Figure 7a). Samples from the Domoni Ridge (MOZ1-DR07 and DR08) also have similar major and trace element compositions, overlapping the field of the Karthala volcano (Figures 2 and 3a). These morphological and geochemical arguments suggest that the Domoni Ridge is a southern extension of the Karthala edifice. Our $^{40}Ar/^{39}Ar$ plateau ages indicate that the Domoni Ridge was active from before 1.4 Ma to at least 1.2 Ma, or even 1 Ma if the pseudo-plateau age of 1.04 ± 0.06 Ma is considered meaningful (Figure 7a). Considering the Domoni Ridge and Karthala as parts of the same structure suggests that volcanic activity initiated along a N150–155°E ridge from the second construction stage of Mohéli (2–0.008 Ma; Rusquet et al., 2023), and gradually concentrated in its northern part from ≥1.4 Ma to the present, building the Karthala volcano.

5.1.2. Activity of Northern Anjouan

Our results also provide information about the history of the construction and destruction of Anjouan. In major and trace elements compositions, the two samples from the submarine northern base of Anjouan (MOZ1-DR09) fall in the fields of the least differentiated rocks from this island (Figures 2 and 3b). Our two $^{40}Ar/^{39}Ar$ ages of

Journal of Geophysical Research: Solid Earth

10.1029/2024JB029488

Table 2

(U-Th)/He Dating Results on Zircon and Apatite Crystals From Volcanic Rocks of the Northern Mozambique Channel

Sample code	LTTF code - grain number	^{232}Th (ng)	± (%)	^{232}Th (ppm)	^{238}U (ng)	± (%)	^{238}U (ppm)	^{147}Sm (ng)	± (%)	^{147}Sm (ppm)	^{4}He (ncc)	± (%)	TAU (%)	Th/U	eU (ppm)	Raw He date (Ma)	±1σ (Ma)	Ft	± (%)	ESR (μm)	Cor. He date (Ma)	±1σ (Ma)	Comment[a]
Zircon																							
SCR-DR09E	V3-1	0.596	2.2	40.4	0.499	2.5	33.8	0.002	11.3	0.2	0.502	1	2.2	1.19	43.3	6.5	0.1	0.84	5	80	7.7	0.4	
SCR-DR09E	V3-2	0.242	2.2	66.2	0.821	2.5	224.7	0.001	16	0.2	27.342	0.4	2.4	0.29	240.3	250.1	6	0.75	5	51	332.6	18.4	Likely inherited
SCR-DR09E	V3-3	0.223	2.2	69	0.409	2.5	126.5	0.001	16.2	0.3	8.571	0.6	2.3	0.54	142.7	150.7	3.5	0.74	5	49	205	11.3	Likely inherited
Fish Canyon Tuff zircon mineral age standard (28.3 ± 1.8 Ma)																							
FCT standard	FCT-23	0.929	2.2	301.6	1.068	2.6	346.6	0.002	10	0.7	3.195	1.9	2.9	0.86	417.4	20.4	0.6	0.73	5	49	27.8	1.6	
FCT standard	FCT-24	0.539	2.2	238.1	0.996	2.5	440.1	0	19.4	0.1	2.978	2	3	0.54	496.1	21.8	0.7	0.71	5	44	30.8	1.8	
FCT standard	FCT-25	0.831	2.3	233.9	1.552	2.6	436.9	0	19.8	0.1	4.659	2	3.1	0.53	491.9	21.9	0.7	0.76	5	53	28.9	1.7	
FCT standard	FCT-26	0.63	2.2	144.4	1.25	2.6	286.5	0	18.1	0	3.839	1.9	3	0.5	320.4	22.5	0.7	0.77	5	55	29.3	1.7	
FCT standard	FCT-27	0.38	2.2	164.5	0.616	2.6	267	0	17.1	0.2	1.771	2.2	3.1	0.61	305.6	20.6	0.6	0.7	5	44	29.3	1.7	
																					Average: 29.1 ± 1.5 Ma		
Apatite																							
SCR-DR01A	V5-1	0.034	5.7	8.2	0.006	5.9	1.4	0.012	0.4	3	0.102	1.1	4.2	5.77	3.3	59.2	2.5	0.72	5	57	82.6	5.4	
SCR-DR01A	V5-2	0.052	4	8.3	0.008	4.3	1.3	0.019	0.4	3.1	0.16	1.4	3.2	6.09	3.3	62.6	2	0.74	5	61	84.9	5.1	
SCR-DR01A	V5-3	0.016	5.7	13.8	0.002	6.1	1.5	0.004	0.7	3.5	0.029	2.8	5.1	9.42	4.7	42	2.2	0.51	10	33	82.8	9.3	
SCR-DR01A	V5-4	0.024	4.1	7	0.006	4.3	1.6	0.009	0.4	2.5	0.067	1.2	3.2	4.21	3.3	47.5	1.5	0.67	5	49	70.5	4.2	
SCR-DR01A	V5-5	0.022	5.7	10.8	0.004	6	1.9	0.007	0.6	3.4	0.048	1.9	4.5	5.61	4.5	43.8	2	0.6	5	40	72.9	4.9	
																					Average: 77.1 ± 2.3 Ma		
Durango apatite mineral age standard (31.8 ± 1.8 Ma)																							
	D-1	0.569	4		0.03	4.2		0.011	0.4		0.608	0.7	3.4	18.74		30.4	1	1	5		30.4	1.8	
	D-2	1.271	5.7		0.068	5.8		0.027	0.3		1.449	0.6	4.8	18.49		32.3	1.5	1	5		32.3	2.2	
	D-3	1.321	4		0.062	4.2		0.03	0.4		1.495	0.6	3.5	21		32.8	1.1	1	5		32.8	2	
	D-4	0.92	5.7		0.053	5.8		0.023	0.4		1.046	0.6	4.7	17.22		31.8	1.5	1	5		31.8	2.2	
	D-5	0.438	4		0.029	4.2		0.009	0.5		0.482	1.5	3.6	15.08		30	1.1	1	5		30	1.8	
	D-6	0.61	5.7		0.036	5.8		0.013	0.4		0.694	0.8	4.7	16.69		31.7	1.5	1	5		31.7	2.2	

Journal of Geophysical Research: Solid Earth

10.1029/2024JB029488

Table 2
Continued

Sample code	LTTF code - grain number	^{232}Th (ng)	± (%)	^{232}Th (ppm)	^{238}U (ng)	± (%)	^{238}U (ppm)	^{147}Sm (ng)	± (%)	^{147}Sm (ppm)	^{4}He (ncc)	± (%)	TAU (%)	Th/U	eU (ppm)	Raw He date (Ma)	±1σ (Ma)	Ft	± (%)	ESR (μm)	Cor. He date (Ma)	±1σ (Ma)	Comment[a]
	DO-1	1.978	4		0.104	4.2		0.037	0.3		2.246	1.5	3.7	18.92		32.4	1.2	1	5		32.4	2	
	DO-3	1.925	5.7		0.104	5.8		0.049	0.4		2.328	1.6	5	18.29		34.2	1.7	1	5		34.2	2.4	
	DO-4	1.287	4		0.074	4.2		0.028	0.4		1.443	1.2	3.5	17.17		31.4	1.1	1	5		31.4	1.9	
	DO-8	0.875	4		0.051	4.2		0.022	0.3		0.988	1.2	3.5	16.89		31.5	1.1	1	5		31.5	1.9	
																					Average: 31.7 ± 1.3 Ma		
Apatite																							
SCR-DR10C	V2-1	0.041	5.8	30.7	0.009	5.9	6.7	0.003	0.6	2.5	0.006	4.1	5.8	4.54	13.9	2.6	0.1	0.58	10	38	4.4	0.5	
SCR-DR10C	V2-3	0.118	4.1	72.4	0.019	4.3	11.3	0.008	0.5	4.9	0.025	4.4	5.3	6.34	28.3	4.4	0.2	0.6	5	41	7.2	0.5	
SCR-DR10C	V2-4	0.233	5.8	56.5	0.061	5.9	14.6	0.024	0.3	5.8	0.141	1.4	4.3	3.83	27.9	10	0.4	0.71	5	55	14	0.9	Outlier (visible inclusion)
SCR-DR10 C	V2-5	0.12	4.1	25	0.015	4.3	3.1	0.008	0.5	1.7	0.024	4	5	7.89	9	4.5	0.2	0.73	5	59	6.2	0.4	
SCR-DR10C	V2-6	0.105	5.8	94.4	0.022	5.9	19.8	0.006	0.5	5.5	0.018	5.8	7.1	4.74	41.9	3.2	0.2	0.51	10	33	6.3	0.8	
SCR-DR10C	V2-7	0.039	4.1	44.9	0.012	4.3	13.8	0.003	0.8	3.1	0.008	4.1	5.1	3.22	24.4	3	0.2	0.52	10	33	5.8	0.6	
																					Average: 6.0 ± 0.3 Ma		
Durango apatite mineral age standard (31.8 ± 1.8 Ma)																							
DO-2	2.017	4.1		0.109	4.2		0.031	0.5		2.148	1.5	3.7	18.42		30.2	1.1	1	5		30.2	1.9		
DO-5	1.068	5.8		0.063	5.9		0.024	0.3		1.191	1.3	4.9	16.81		31.1	1.5	1	5		31.1	2		
DO-6	2.026	4.1		0.107	4.3		0.038	0.5		2.234	1.4	3.7	18.77		31.4	1.2	1	5		31.4	2		
																				Average: 30.8 ± 2.3 Ma			

Note. TAU-total analytical uncertainty; eU - effective uranium concentration (eU = [U] + 0.235[Th]); Raw He age - (U-Th)/He date uncorrected for alpha ejection; Ft - alpha ejection correction factor calculated after Farley et al. (1996) for homogeneous distribution of parent nuclides; ESR - equivalent sphere radius; Cor. He age - (U-Th)/He date corrected for alpha ejection. [a]Analysis disregarded for the reason given in the "Comment" column.

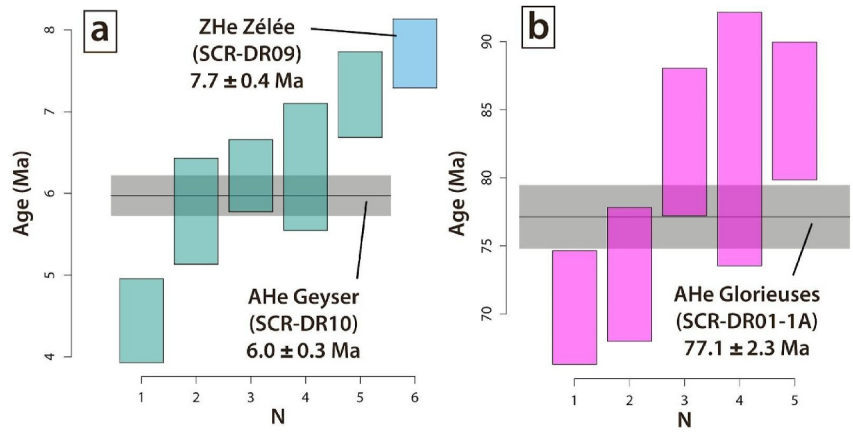

Figure 6. Ranked order plots of (U-Th)/He dates on zircon (ZHe) and apatite (AHe) crystals, displayed as 1σ error bars, with weighted mean values and 1σ uncertainties. (a) Zélée and Geyser banks. (b) Seamount from the Glorieuses chain. Note that two anomalously old ZHe dates are not displayed for clarity purposes.

0.95 ± 0.06 Ma and 0.94 ± 0.09 Ma agree with the two K-Ar ages of 0.899 ± 0.014 Ma and 0.808 ± 0.012 Ma obtained on the subaerial northern massif of Anjouan (Quidelleur et al., 2022), illustrating the consistency of the $^{40}Ar/^{39}Ar$ and K-Ar techniques when applied to carefully selected rocks (Figure 7a).

Anjouan Island is made of two rift zones oriented N110°E and N150°E (Famin et al., 2020), the northern base dredged by MOZ1-DR09 belonging to the latter structure. On the one hand, the N110°E rift zone likely corresponds to the early volcanism of Anjouan, because it follows the tip of the ca. 4 Ma Chistwani Ridge (Rusquet et al., 2023). The N110°E rift zone became subaerial at ca. 1.5 Ma and remained active until ca. 0.5 Ma according to K-Ar groundmass ages and retained K-Ar whole rock ages (Quidelleur et al., 2022). On the other hand, the N150°E rift zone is the most recently active structure as shown by the alignment of uneroded volcanic cones and craters (Quidelleur et al., 2022). New submarine $^{40}Ar/^{39}Ar$ ages and published subaerial K-Ar ages show that this N150°E structure has been built since at least ca. 0.9 Ma and remained active until Holocene times. Incidentally, new results confirm that the landslide that dissected the northern side of Anjouan is more recent than 0.9 Ma (Figure 7a), as proposed by Quidelleur et al. (2022). Taken together, relative and absolute geochronological criteria suggest that the volcanic construction of Anjouan involves the N110°E axis from 4 to 0.5 Ma, an emersion at >1.5 Ma, and a progressive concentration of activity along the N150°E axis from 0.9 to 0 Ma.

5.1.3. Subaerial History of Mayotte

In this section, we combine new and published data to refine the geological history of Mayotte. Compared to the other volcano-tectonic structures of the northern Mozambique Channel, the data set for Mayotte is much larger and includes 58 ages, 34 of which are K-Ar whole rock ages (Emerick & Duncan, 1982, 1983; Hajash & Armstrong, 1972; Nougier et al., 1986), and 24 are $^{40}Ar/^{39}Ar$ ages on groundmass (Pelleter et al., 2014). Additional $^{40}Ar/^{39}Ar$ and K-Ar ages are also available in an unpublished thesis (Debeuf, 2004), but these ages have been discarded in the publication derived from the thesis (Pelleter et al., 2014) and will hence not be considered further here. As a general observation, many of the ages do not satisfy the quality criteria inherent in each dating technique, have large uncertainties, and/or contradict each other. We therefore applied a filtering procedure and a cross-comparison of published and new ages to build a robust age database for Mayotte. The filtering methodology and the cross-comparison are provided in Supporting Information S1. From the initial database, 11 published ages can be considered as reliable (K-Ar on whole rock and $^{40}Ar/^{39}Ar$ on groundmass), 33 ages (K-Ar on whole rock and $^{40}Ar/^{39}Ar$ on groundmass) are rejected by the filtering procedure, and we keep 14 K-Ar whole-rock ages that could not be evaluated, even though these ages might be prone to inaccuracy as already shown for Anjouan (Quidelleur et al., 2022) and Mohéli (Rusquet et al., 2023). Considering the 4 groundmass K-Ar ages from this study and the 25 remaining literature ages, we retain a total set of 29 new and previously published radiometric ages for subaerial Mayotte lavas for interpretation purposes (Figure 7b; Table 1, S3 in Supporting Information S4). Seismic profile interpretations (Masquelet et al., 2022) and the age-probability calculated from radiometric data suggest that the volcanic construction of Mayotte Island may be summarized

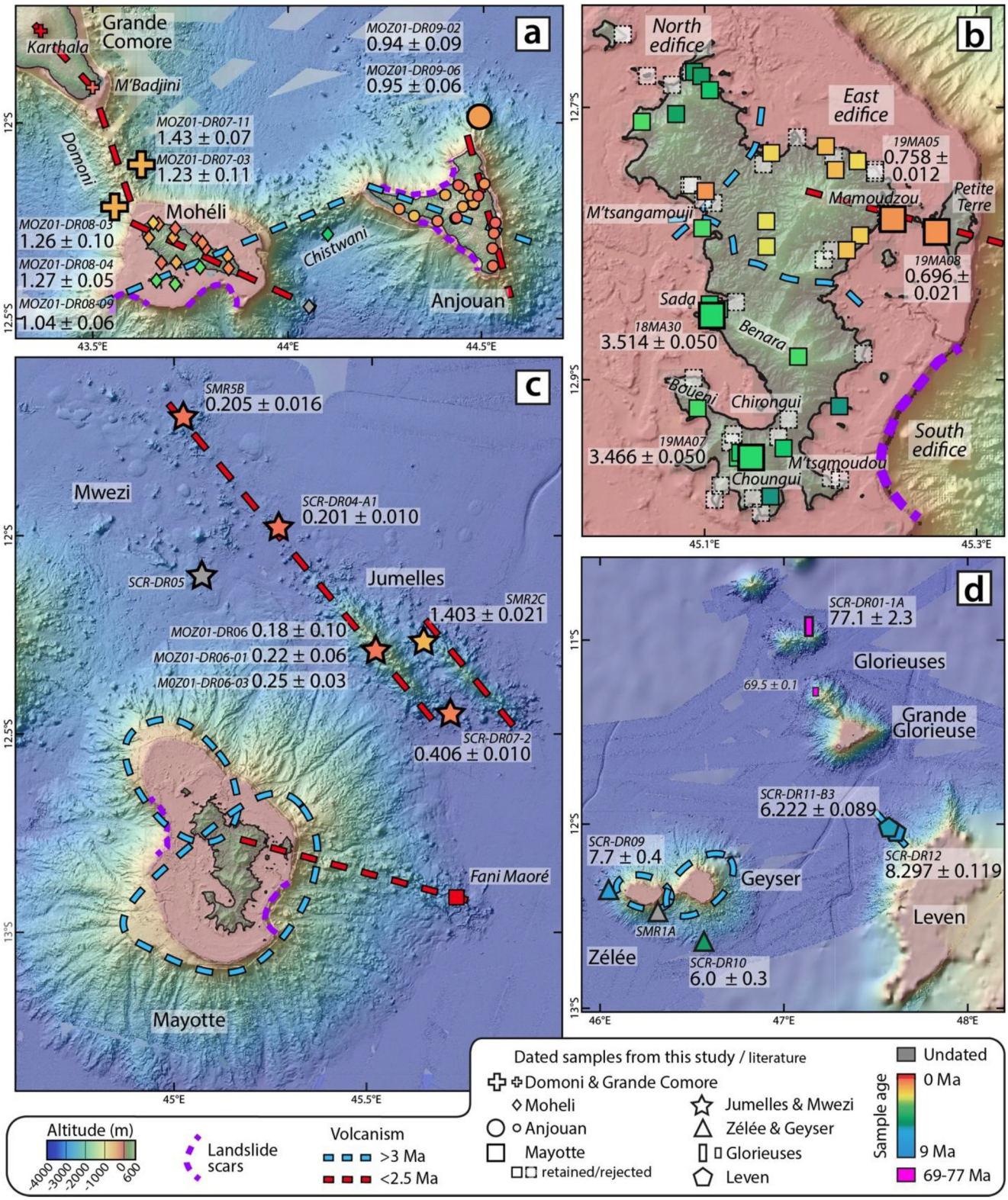

Figure 7.

as follows (Figure 8). Early submarine construction of southern and north-eastern Mayotte initiated at 27–26 Ma and resumed sporadically in Mayotte north-east and north. From at least 6 Ma to 4.6 Ma, two subaerial edifices coexisted, a south volcano and a north-west volcano with mostly mafic products. After an apparent quiescence of ~1 Myrs, volcanic activity resumed on these two eruptive centers from 4 to 3.2 Ma with more evolved magmas (Figures 2 and 3c), infilling previously incised valleys and yielding inverted topography. Then, a lack of ages between 3.2 and 2.4 Ma suggests a period of volcanic hiatus and erosion on Mayotte in this time interval. Importantly, the south flank of the south volcano and the western flank of the north-west volcano both display submerged reef platforms subsided to depths of 400–800 m, whereas the more recent submarine morphologies do not show any subsided relief (Figure 7c). This implies that the 3.2–2.4 Ma period of volcanic hiatus and erosion corresponds to a subsidence of the two coalesced volcanoes. Interestingly, the location and shape of these drowned platforms suggest that the Mayotte south edifice had a SW-NE oblong shape whereas the north-west edifice was slightly elongated in the NW-SE direction (Figure 7c). Platforms also drowned in Mohéli between 3 and 2 Ma, suggesting that the subsidence was regional.

The next volcanic renewal occurred on a new eruptive center east of the north-west edifice from 2.4 to 1 Ma, along a N110°E axis (Figures 7b and 7c). Erupted products at this stage are moderately undersaturated (Figure 2). Then, after an apparent hiatus of 0.2 Ma, activity resumed on this edifice, with Strombolian mafic volcanism on the north-east of Mayotte from 0.8 to 0.7 Ma. The most recent volcanic history of Mayotte propagates to the east along the N110°E axis, with explosive phonolitic volcanism of Petite Terre at ≥25 ka (Lacombe et al., 2024), followed by offshore activity and the emplacement of the 2018–2021 Fani Maoré submarine volcano (Bazin et al., 2022; Lemoine et al., 2020, Figure 7c).

5.1.4. Construction of the Jumelles Ridges and the Mwezi Volcanic Province

The morphology of the Mwezi volcanic province is a N130°E lineament of monogenic seamounts and domes extending north of the two Jumelles polygenic ridges, almost aligned with the N135°E western ridge (Thinon et al., 2022). Our geochemical and geochronological data provide constraints on the nature and temporality of volcanism in this area. All the samples from the Jumelles ridges and the Mwezi volcanic province are characterized by basaltic to tephritic-basanitic major element compositions (Figure 2), and trace elements patterns representative of Comorian lavas (Figures 3d and 4). These morphological and geochemical features suggest that the Jumelles and the Mwezi volcanic province have a common volcano-tectonic origin. In detail, however, the Jumelles ridges have higher incompatible trace element concentrations than the Mwezi province (Figure 3d), indicating more evolved magma compositions in the former case.

The three $^{40}Ar/^{39}Ar$ whole rocks ages and three K-Ar groundmass ages of the Jumelles ridges and the Mwezi volcanic province represent the first radiometric dating results on these submarine volcanic features (Figure 7c). The K-Ar age of 1.403 ± 0.021 Ma at the northern tip of the eastern ridge (SMR2) is located at the base of this edifice, and is thus possibly related to the early construction of the Jumelles ridges. This is confirmed by the dredge content of carbonate fragments and Fe-Mn oxide concretions in addition to pillow lavas of olivine basalt (Thinon et al., 2021), implying an exposure long enough for sedimentation and oxide precipitation. In comparison, the dredge at the southern tip of the western Jumelle (SCR-DR07) contained only pillows of fresh aphyric basalt without any sedimentary or oxide deposits, consistent with the much younger age of 0.406 ± 0.010 Ma obtained by K-Ar on groundmass. For the dredge on the upper slopes of the western Jumelle (MOZ01-DR06), we choose to merge the three $^{40}Ar/^{39}Ar$ ages at 0.25 ± 0.03, 0.22 ± 0.06, and 0.18 ± 0.01 Ma into a single weighted mean age of 0.24 ± 0.026 Ma, because of their similar major-trace element compositions and their overlapping uncertainties. Overall, absolute ages and relative chronological criteria thus both show that the zones dredged by MOZ01-DR06 and SCR-DR07 are younger than the SMR2 area. This implies a history of protracted mafic volcanic activity on the two Jumelles ridges from >1.4 Ma to less than 0.2 Ma.

Figure 7. Radiometric ages (in Ma) reported on topographic and bathymetric maps. (a) Grande Comore south (including Karthala active volcano), Domoni Ridge, Mohéli, and north Anjouan, with dredged sites. (b) Subaerial Mayotte with a comparison of new and published radiometric ages. The subaerial part of the island is subdivided into three edifices based on morphologies and radiometric ages (Pelleter et al., 2014): Mayotte south and Mayotte north-west are two edifices >3 Ma displaying eroded morphologies and inverted topography, whereas Mayotte north-east is <2.5 Ma and displays a shield shape with less eroded slopes. (c) Mayotte (including Fani Maoré active submarine volcano), Jumelles ridges, and Mwezi volcanic province. Note the N110°E and N140°E elongation of volcanic structures in this area. (d) Leven Bank, at the junction of the N150°E alignment of the Glorieuses seamounts and the E-W alignment of the Comoros Archipelago and Zélée-Geyser banks. Blue dashed lines and ellipses correspond to volcanic structures older than 3 Ma whereas red dashed lines highlight structures younger than 2.5 Ma.

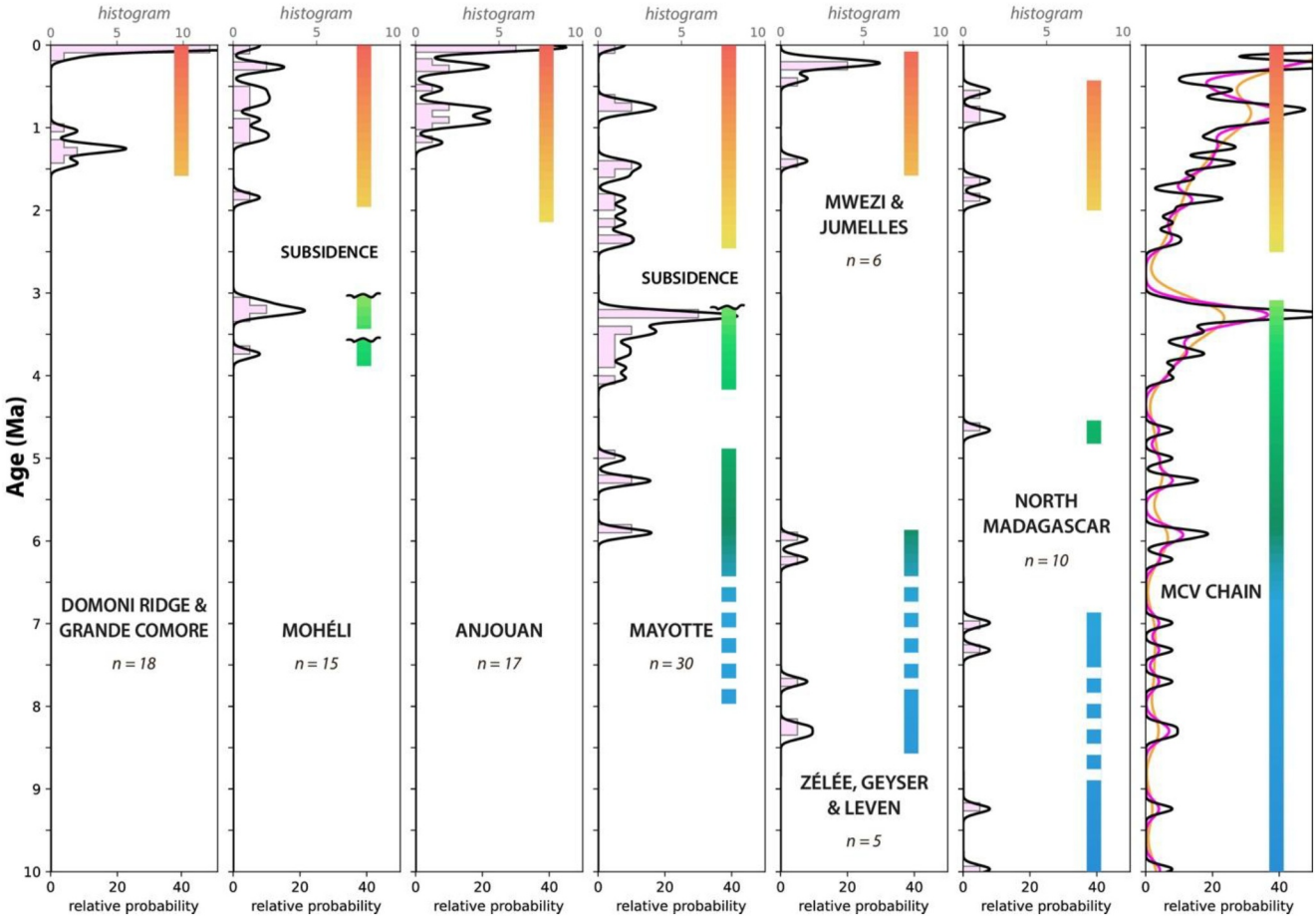

Figure 8. Age probability plots (histograms and Kernel density estimates with bandwidths of 50, 100, and 200 kyrs in black, purple, and orange, respectively) and chronostratigraphy of volcanic structures from the Comoros Archipelago and northern Madagascar since 10 Ma. Ages data set given in Table S4. The color chart corresponds to ages of volcanism as in Figures 1–7.

The two K-Ar groundmass ages of the Mwezi province at 0.205 ± 0.016 and 0.201 ± 0.01 Ma come from dredges located on two volcanic seamounts, which recovered only aphyric basalt pillow lavas in SCR-DR04, and popping basalt pillow lavas mixed with unconsolidated carbonate mud in SMR5 (Thinon et al., 2021). Volcanic products were also recovered by dredge SCR-DR05 on another seamount, but these materials were not fresh enough to be dated.

Taken together, results imply that the Jumelles ridges and the Mwezi province represent a continuous zone of volcanic seamounts aligned in a N130-N135°E fashion (Figure 7c), with intermittent mafic activity in the interval >1.4–0.2 Ma (Figure 8). The decreasing ages from the Jumelles ridges to Mwezi, the less-evolved compositions of magmas in the latter, the decreasing height of edifices from the SE to the NW, and the changing volcanic morphologies from polygenic to monogenic, all suggest that the Mwezi province is a propagation of the Jumelles volcano-tectonic structures toward the NW.

5.1.5. Activity of the Zélée and Geyser Banks

Does the volcanism of the Zélée and Geyser banks belong to the Comoros Archipelago? The Zélée and Geyser banks are two coalesced elliptical edifices roughly aligned in the E-W direction (Figure 7d). In detail, however, (a) the sharp N070°E western edge of the Geyser Bank suggests that this edifice was in fact a SW-NE oblong structure as for early Mohéli and Mayotte south and (b) the Zélée Bank presents a N110°E orientation similar to the western rift zone of Anjouan. The recovery of foïdites and basalts (Figure 2), albeit altered, on the three dredges of the Zélée and Geyser banks (SMR1, SCR-DR09, and DR10) implies that highly and moderately silica-undersaturated magmas coexisted during construction of the edifices, a pattern also shared by Mohéli and

Mayotte (Pelleter et al., 2014; Rusquet et al., 2023). The similarity is also highlighted by immobile trace element ratios, Zélée and Geyser showing La/Yb values at given Nb/Zr in the upper range of Comorian lavas, as for some of Mayotte's data and unlike the Jumelles-Mwezi structures (Figure 4). The morphology and geochemistry of the Zélée and Geyser banks are thus comparable to the oldest volcano-tectonic structures of the Comoros Archipelago (Mohéli and Mayotte). Our ZHe age of the eastern base of Zélée at 7.7 ± 0.4 Ma and the AHe age obtained on the south flank of Geyser at 6.0 ± 0.3 Ma document a protracted activity of these seamounts in the 8–6 Ma interval, slightly preceding the emersion of Mayotte's south volcano (Figure 8). These ages confirm that the Zélée and Geyser banks, together with Mayotte, are the oldest edifices of the Comoros Archipelago.

5.1.6. The Glorieuses Alignment

It is also important to discuss whether the Comoros Archipelago and the Glorieuses alignment share similar magmatic sources and/or timing of volcanic activity. The silica-saturated trend in the TAS diagram up to the trachyte field (Figure 2), the elevated concentrations of some incompatible elements (Dy to Lu in SCR-DR01-1A and 1B or Ta, Ce, Pr, Zr, and Nd in the other samples) compared to the Comoros (Figure 3f), and the absence of correlation among immobile trace element ratios (Figure 4) all indicate that the Glorieuses alignment of seamounts and islets has a very distinct major and trace element signature from the Comorian volcanism, calling for different melting sources and/or ascent processes. Leroux et al. (2020) placed the volcanic construction of Grande Glorieuse Island in the Late Cretaceous, with two magmatic pulses during the Turonian and the Maastrichtian. Our AHe age of 77.1 ± 2.3 Ma further shows that the construction of the seamount north of Grande Glorieuse also occurred in the Campanian, thus confirming the formation of the Glorieuses alignment in the Late Cretaceous, well before the initiation of Cenozoic volcanism in the Comoros and northern Madagascar. Geochemical and geochronological data thus indicate that the construction of the N160°E trend of the Glorieuses and the E-W alignment of the Comoros are the results of totally independent magmatic episodes, the former being at least 40 Myrs older than the latter.

5.1.7. Does the Leven Bank Belong to the Comoros or to the Glorieuses Trends?

The major and trace element signature of the Leven Bank lavas, and in particular their immobile trace-element patterns, is consistent with those for volcanic products from the Comoros and the Cenozoic volcanism of northern Madagascar, but strikingly different from the signature of the Glorieuses trend (Figures 2, 3f, 4). These similarities and differences are also reflected in the geochronological record. Indeed, the basanite dredged on a N160°E submarine ridge dated at 8.30 ± 0.12 Ma (SCR-DR12), and the tephrite/basanite dredged on a seamount dated at 6.22 ± 0.09 Ma (SCR-DR11), suggest that the Leven Bank remained a zone of intermittent volcanic activity for a protracted period between 8.5 and 6 Ma. The important consequence of these Late Miocene ages is that the tip of the Leven Bank, whose volcanic nature is confirmed by our study, was coeval with the activity of Zélée–Geyser (8–6 Ma) and Mayotte south (>6 Ma), and experienced volcanism much later than the Cretaceous volcanism of the Glorieuses seamounts. Leroux et al. (2020) reported a period of uplift of Grande Glorieuse at 9.5–8.9 Ma, much later than its magmatic activity, which we interpret as related to the volcanism of the nearby Leven Bank at that time. Thus, radiometric ages and trace-element compositions unambiguously demonstrate that the volcanism of the Leven Bank belongs to the Comoros volcanic chain and not to the Glorieuses alignment.

5.2. Integration of the Volcanism of the Comoros at a Regional Scale

5.2.1. Comparison With the Volcanism of Northern Madagascar

With the inclusion of new dates for the Jumelles, Zélée, Geyser, and Leven banks into the volcanism of the Comoros, we interpret this set of volcanic structures as an E-W alignment that structurally and magmatically connects to the Cenozoic volcanism of northern Madagascar (Bobaomby Peninsula, Massif d'Ambre, and Nosy Be–Ankify area). Cucciniello et al. (2022), Melluso and Morra (2000), and Rusquet et al. (2023) noted the similarities of trace element and Sr-Nd-Pb signatures among the volcanic products of Grande Comore, Mohéli, Mayotte, and Cenozoic northern Madagascar. New trace element results show that such similarities may be extended to Anjouan, the Jumelles ridges, the Mwezi province, and the Zélée, Geyser, and Leven banks, excluding the Cretaceous volcanism of the Glorieuses (Figures 3 and 4). Thus, trace element concentrations suggest that Comorian and northern Madagascar melts share similarities in mantle sources and/or ascent processes in the lithosphere. This evidence supports the idea that the Comorian volcanism is spatially and chemically

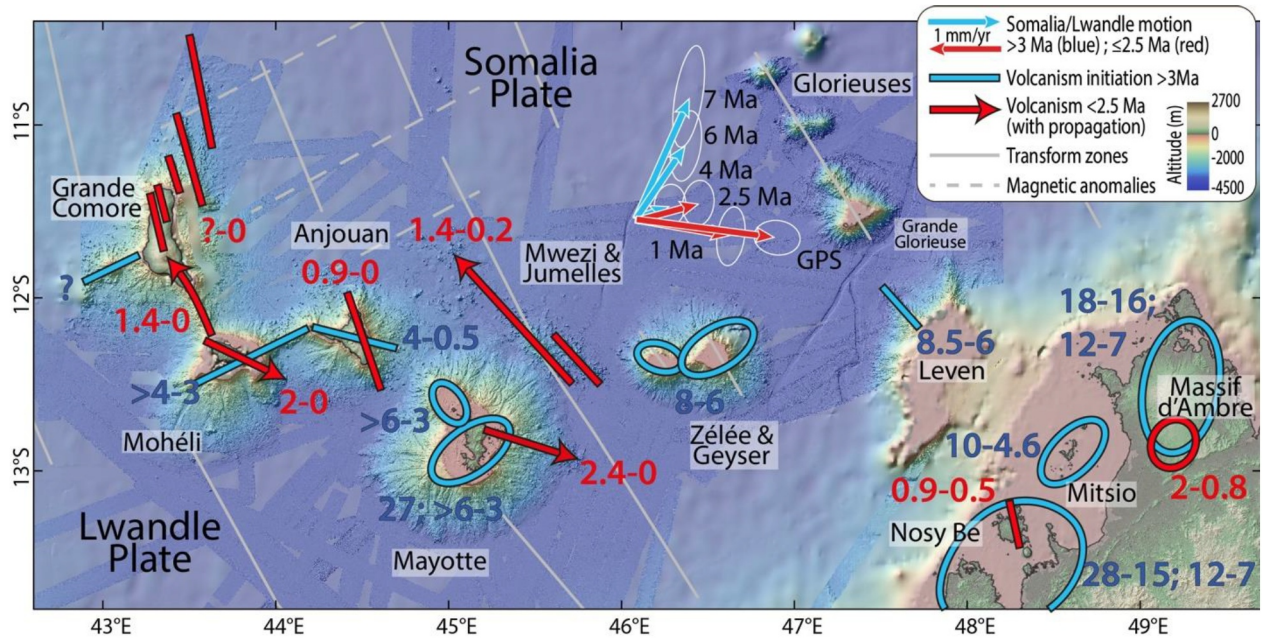

Figure 9. Synthesis map of Cenozoic volcanic activity in the northern Mozambique Channel before 3 Ma (in blue) and after 2.5 Ma (in red, sometimes with propagation symbolized with arrows). Volcanic structures are represented as segments when their orientation is identified, as ellipses otherwise, with corresponding phases of activity (in Ma). Also shown are motion vectors of the Somalia plate relative to the Lwandle plate at an arbitrary location on the Somalia plate (lat. −11.6°, long. 46.1°), before 3 Ma (7.5, 6, and 5.2 Ma, in blue) and after 2.5 Ma (2.5, 0.8, and average GPS data, in red). See text and Figure 10 for calculation details. Transform zones (solid gray lines) and magnetic anomalies (dashed gray lines) are from Phethean et al. (2016).

connected to the Cenozoic volcanism of northern Madagascar. The question thus arises as to whether the temporality of volcanism confirms this connection.

Unfortunately, geochronological constraints remain sparse in northern Madagascar, which limits any temporal comparison with the Comoros volcanism to a rough evaluation. The earliest Cenozoic volcanism documented at 28–27 Ma in the Ankify Peninsula (Buchwaldt, 2006) is comparable with interpretations of seismic profiles placing the initiation of Mayotte's volcanism at 27-26 Ma (Masquelet et al., 2022). There is also evidence of sporadic volcanic activity all over northern Madagascar in the interval 28–15 Ma (Buchwaldt, 2006; Cucciniello et al., 2011; Emerick & Duncan, 1982, 1983; Estrade et al., 2014; Tucker et al., 2008). The geochronological record allows more detailed comparisons over the past 10 Ma (Figure 8). Volcanism is documented at 12–17 Ma in the Bobaomby Peninsula, in the Massif d'Ambre, in the Mitsio islands, and in Nosy Be (Buchwaldt, 2006; Cucciniello et al., 2011; Emerick & Duncan, 1982, 1983), while there is magmatism on Mohéli and Mayotte islands at prior to 6 Ma, on the Zélée and Geyser banks at 8–6 Ma, and on the Leven Bank at 8.5–6 Ma. Then, after an apparent 2.3 Myrs hiatus, one age at 4.66 ± 0.12 Ma is documented in the Mitsio islands (Emerick & Duncan, 1982, 1983), indicating a volcanism contemporaneous of the two subaerial edifices in Mayotte south and north (6–4.6 Ma). No radiometric dates exist in northern Madagascar in the 4.6–2 Ma interval, whereas Mayotte and Mohéli islands are both active between 4 and 3 Ma (Debeuf, 2004; Nougier et al., 1986; Pelleter et al., 2014; Rusquet et al., 2023), and volcanism initiates on Anjouan Island at 4–1.5 Ma. A widespread volcanic renewal occurs in Massif d'Ambre and Nosy Be since 2 Ma (Bardintzeff et al., 2010; Emerick & Duncan, 1982, 1983; Tucker et al., 2008), coeval with the widespread activity of the Domoni Ridge (Grande Comore), Mohéli, Anjouan, Mayotte, and Jumelles–Mwezi in the last 2.4 Ma (Figure 8). Thus, the available geochronological constraints indicate repeated volcanic activity in the Comoros and northern Madagascar since 10 Ma, and possibly since 28 Ma. As a consequence of these spatial, chemical, and temporal similarities, we interpret the Cenozoic volcanism of northern Madagascar and the Comoros Archipelago as belonging to the same E-W, 700-km-long and 200-km-wide chain of volcanoes, connected by the Zélée, Geyser, and Leven banks (Figure 9).

Considering the north Madagascar–Comoros volcanic (MCV) chain as a single E-W lineament has implications for the contentious question of a westward progression of volcanism in relation to the hotspot or plate boundary hypotheses. As mentioned above, seismic profile interpretations and radiometric ages suggest that the Comorian

volcanism initiated in Mayotte at 27–26 Ma (Masquelet et al., 2022) and in Domoni-Grande Comore at 1.4 Ma, suggesting a westward propagation. Including northern Madagascar's magmatism at ca. 28 Ma neither confirms nor refutes this apparent westward younger age progression, keeping in mind that geochronological data are sparse in northern Madagascar and that older volcanic ages may be found in future studies. Looking at radiometric ages only (new and published), a second westward age progression of volcanism might be seen from 10 to 17 Ma in northern Madagascar to 8.5–6 Ma in the Leven Bank, 8–6 Ma in the Zélée-Geyser banks, 6–3 Ma in Mayotte, 4–3 Ma in early Mohéli, and 1.4 Ma in Grande Comore (Figure 8). Regardless of the existence of an age progression, the combined geological information (geochemistry, ages, observed unconformities and erosion separating units, eustatic variations of Grande Glorieuse, Mayotte, and Mohéli) shows that sporadic volcanism occurred all over the MCV chain since at least 28 Ma, among which two phases of activity are prominent since the Late Miocene. The first phase initiates with the uplift of the Glorieuses 9.5–8.9 Ma (Leroux et al., 2020) and the activation of many eruptive centers at 9–8 Ma and until no later than 3 Ma (Nosy Be, Massif d'Ambre, Leven, Geyser-Zélée, Mayotte, Mohéli) along both NE-SW and NW-SE structures (Figures 8 and 9). After this magmatic event, the subsidence of islands and the hiatus of volcanism suggest an interruption of magma supply along the MCV chain from 3 to 2.5 Ma. Then, a second phase of activity occurs from 2.5 Ma and consists of volcanic renewal (Nosy Be, Massif d'Ambre), the reorientation of preexisting structures (Mayotte, Mohéli, and Anjouan), and the birth of new structures (Jumelles-Mwezi, Domoni-Grande Comore). This latter phase leads to the widening of the MCV chain, mostly toward the north with the propagation of volcanism from the Jumelles ridges to the Mwezi province, and from the Domoni Ridge to Karthala volcano (Figure 9). In this latest phase, volcano-tectonic structures are systematically oriented NW-SE and arranged in an en-échelon fashion (Famin et al., 2020; Feuillet et al., 2021; Thinon et al., 2022).

5.2.2. Dynamics of the MCV Chain in the Framework of Plate Kinematics

The recurrence of volcanism at different localities along the MCV chain since at least 28 Ma, with no obvious age progression, is difficult to fit in the framework of a hotspot model, even if it does not completely rule out this possibility. Moreover, the two widespread magmatic reactivations at 9–8 and 2.5 Ma are even more difficult to explain with the hotspot trail hypothesis, as is the expansion of the zone of active volcanism toward the north since 2.5 Ma (Figure 9). Conversely, phases of magmatism and tectonics, and propagating volcanism, are characteristic features of widening extension in the lithosphere, as for instance described in several segments of the EARS including the Rungwe Volcanic Province, the Northern Tanzania Divergence, the Southern Kenya Rift, and the Turkana Broadly Rifted Zone further north (Ebinger et al., 2000; Mana et al., 2015; Martin, 2023; Rooney, 2020). A consensus is slowly emerging that the Comoros may connect to Madagascar and the EARS, forming an E-W boundary between the Lwandle and Somalia plates according to earthquake catalogs and field-observed deformation (Famin et al., 2020; Michon, 2016; Michon et al., 2022; Stamps et al., 2018). Consequently, we interpret the repeated volcanism of the MCV chain, the regional synchronous reactivations of magmatic centers, and the widening volcanism as evidence of the maturation of an E-W zone of lithospheric deformation and magmatism corresponding to the northern segment of the "Indian Ocean branch" of the EARS (Michon et al., 2022). This lithospheric deformation and magmatism may be influenced by a mantle plume, as suggested by seismic tomographic evidence of mantle upwelling in the northern Mozambique Channel (e.g., Boyce et al., 2023; Dongmo Wamba et al., 2023).

The critical question that arises from interpreting the MCV chain as a zone of lithospheric deformation is whether its geodynamic evolution is consistent with plate kinematics. On the first order, the seafloor spreading history of the Southwest Indian Ridge indicates that Lwandle–Antarctica plate motion has closely tracked Somalia–Antarctic plate motion since 50 Ma, suggesting slow-to-no motion between the Lwandle and Somalia plates for much of that time (DeMets et al., 2015, 2021). In detail, however, stage velocities of the Somalia plate relative to the Lwandle plate, calculated by combining Lwandle/Antarctica and Somalia/Antarctica noise-reduced finite rotations (Table 6 and 9 in DeMets et al., 2021), display slight temporal variations. These variations, represented in Figure 10 by calculating the velocity of Somalia relative to Lwandle at an arbitrary location on the Somalia plate, include two velocity increases since the Late Miocene, one at 8–7.5 Ma and another one since 2.5–2 Ma (Figure 10a). These two velocity increases are contemporaneous within 0.5 Ma of the two most recent magmatic renewals of the MCV chain. Changes in the azimuth of the Somalia plate stage velocities relative to the Lwandle plate also slightly exceed 1σ uncertainties, from ≤50°N in the Late Miocene to ≥70°N since the Pleistocene, the latter being consistent with GPS plate motion models (Figure 10b). Considering the MCV chain as the E-W

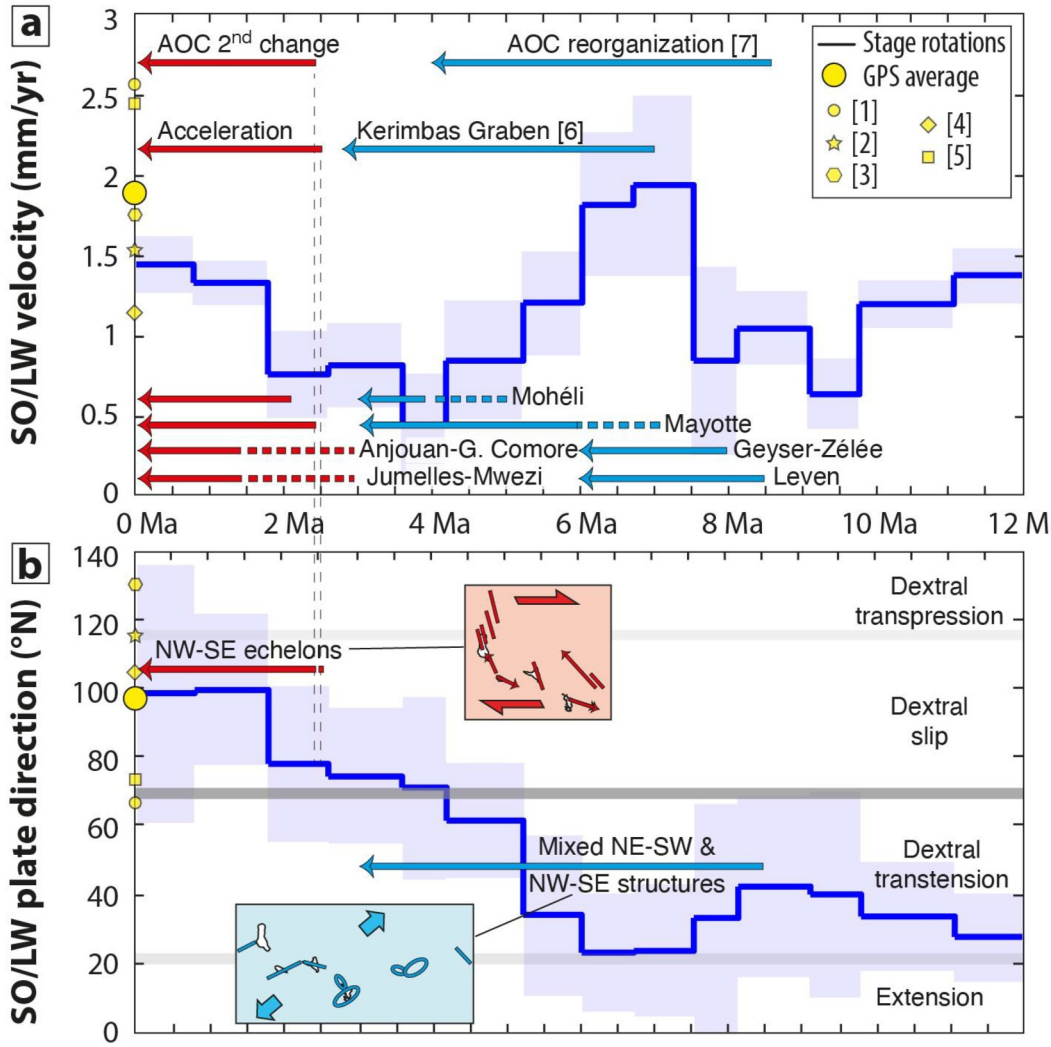

Figure 10. (a) Magnitude and (b) azimuth of Somalia plate (SO) motion vectors relative to the Lwandle plate (LW), calculated at an arbitrary location on the Somalia plate (lat. −11.6°, long. 46.1°). Temporal variations are calculated by combining noise-reduced Lwandle/Antarctic and Somalia/Antarctic finite rotations (Tables 6 and 9 in DeMets et al., 2021). Uncertainties at the 1σ level are calculated by summing the coefficients of covariances matrices of Lwandle/Antarctica and Somalia/Antarctica stage angular velocities (Tables 7 and 10 in DeMets et al., 2021). Present-day motion vectors and their average are calculated from GPS-derived plate models ([1] GEODVEL, Argus et al., 2010; [2] GRSM v2.1, Kreemer et al., 2014; [3] Saria et al., 2014; [4] Graham et al., 2018 [5] T25 M, Wang et al., 2018). Figure 10b is subdivided into four deformation regimes (extension, transtension, strike-slip, and transpression) assuming an E-W Lwandle/Somalia plate boundary. The insets in Figure 10b represent the structures of the Comoros Archipelago before 3 Ma and after 2.5 Ma, as drawn in Figure 9. Also represented are the main volcanic phases of the northern Madagascar-Comoros volcanic chain, and the main tectonic and magmatic changes at the boundaries of the Lwandle and Somalia plates ([6] Kerimbas Graben, Franke et al., 2015 [7] Aden-Owen-Carlsberg -AOC- triple junction, Rodriguez et al., 2018).

trending northern boundary between the Lwandle and Somalia plates, such a velocity reorientation imposed a change in the kinematics of this frontier, from oblique extension in the Late Miocene–Pliocene, to pure dextral strike-slip since the Pleistocene (Figures 9 and 10b). This transition may explain why the MCV chain evolved from a mixed set of NW-SE and NE-SW volcano-tectonic structures compatible with a dextral transtension stress state in the Miocene-Pliocene, to a conspicuous array of en-échelon NW-SE ridges typical of a dextral slip stress state since the past 2.5 Ma (Figures 9 and 10b). Some of these volcano-tectonic structures might reactivate the fabric of the oceanic lithosphere, such as the N070°E Mohéli-Chistwani Ridge, and the N150°E rift zone of Anjouan (Figure 9). The reorientation of volcano-tectonic structures is thus consistent with regional tectonic stress changes in a preexisting lithospheric fabric. In this interpretation, the accumulated load of volcanic edifices

on the oceanic lithosphere is not considered, although it may also have generated stress rotations impacting the orientation of volcano-tectonic structures, as in the East African Rift (Oliva et al., 2022).

Importantly, several modifications of the Lwandle, Rovuma, and Somalia plate boundaries occurred since the Late Miocene. South of the Comoros Archipelago in the Mozambique Channel, along the possible boundary between the Rovuma and Lwandle plates, lie a series of Oligocene NE-SW- and NW-SE-oriented volcano-tectonic structures (i.e., Hall and Jaguar banks, Bassas da India atoll, Ptolémée seamount, and Europa Island) reactivated from 9 to 8 Ma to the Pleistocene (Berthod et al., 2022a). Further north along the Rovuma/Lwandle boundary, there is evidence of tectonic reactivation and volcanism renewal along the Davie fracture zone since the Late Neogene (Figures 1a, Courgeon et al., 2016, 2018; Deville et al., 2018). Along the boundary between the Rovuma and Somalia plates, another important change is the initiation of the Kerimbas Graben at ∼7 Ma (Figures 1a and 10a), and especially its drastic acceleration in rate of opening since the Pleistocene (2.5 Ma), which is responsible for ∼80% of the extension in this area (Table 1 in Franke et al., 2015). Lastly, a major change occurred in the geometry of the Aden-Owen-Carlsberg (AOC) triple junction between Somalia, Arabia, and India at ∼8 Ma (Figures 1a and 10a), affected by a series of structural adjustments (Rodriguez et al., 2018). This geometry change may be linked to the deceleration of the Somalia/Antarctica spreading rate at the same time (DeMets et al., 2015, 2021). A second change in the AOC occurs since 2.4 Ma (Figure 10a), with the opening of the Beautemps-Beaupré basin (Rodriguez et al., 2018).

All these lines of evidence clearly indicate changes in the kinematics of the Lwandle-Rovuma-Somalia plate system at 9–8 Ma and since ∼2.5 Ma (Figure 10). We therefore conclude that the two Late Miocene phases of generalized magmatic activity along the MCV chain, and the reorientation of volcano-tectonic structures from the first phase to the second, are most likely part of the Lwandle and Somalia plate kinematic readjustments at this time. We note that these two most recent magmatic reactivations of the MCV chain coincide with the plate kinematic changes and the geometric modifications of boundaries (Figure 10), further calling for an influence of widespread magmatism on plate motion in the western Indian Ocean as for the rest of the EARS (Michon et al., 2022).

Northwest of the MCV chain and in the westward extension of the Kerimbas Graben, the Rungwe Volcanic Province, the Northern Tanzania Divergence and the Southern Kenya Rift are possible boundaries between the Nubia, Victoria, Somalia, and Rovuma plates (e.g., Saria et al., 2014; Stamps et al., 2018), and the closest volcanic segments of the EARS to the study area (Figure 1a). Do these provinces record magmatic or tectonic events at 9–8 Ma and since 2.5 Ma as the MCV chain, in possible connection with plate kinematics changes and/or fluctuations of mantle upwelling? With our improved history of tectonics of the northern Mozambique Channel, the subject is now ripe for a detailed re-investigation of magmato-tectonic events at plate boundaries over the past 10 Ma in East Africa, considering the MCV chain as a branch of the EARS.

6. Conclusion

New major and trace elements analyses and radiometric dating using multiple techniques on submarine and subaerial volcanic samples from the Comoros Archipelago and the northern Mozambique Channel allow us to draw the following conclusions about the geodynamics of this region since the Late Miocene.

1. The N155°E Domoni Ridge is an early submarine rift zone of the active Karthala volcano in Grande Comore. The Domoni Ridge was active from earlier than 1.4 to ∼1 Ma, suggesting a northward propagation of volcanism from Mohéli to Grande Comore.
2. The northern submarine tip of the N150°E rift zone of Anjouan Island exhibits similar chemical compositions and radiometric ages as the subaerial part of the rift zone. The N110°E rift zone of Anjouan is probably the oldest (4–0.5 Ma) while the N150°E rift zone is the most recently active (0.9–0 Ma). This suggests a reorientation of volcano-tectonics from N110°E to N150°E in the last 0.9 Ma.
3. The subaerial history of Mayotte consisted of the coeval construction of two edifices oriented NE-SW and NW-SE from over 6 to 3.2 Ma. The activity of these two volcanoes ceased from 3.2 to 2.4 Ma, causing a subsidence that drowned carbonate platforms in this interval. Then, activity resumed along a N110°E ridge 2.4 Ma ago, merging the two earlier volcanoes and propagating volcanism eastward through the East-Mayotte ridge and up to the presently active Fani Maoré submarine volcano.
4. The submarine Jumelles ridges and the recently discovered Mwezi volcanic province are parts of the same N135°E volcano-tectonic structure, of chemical composition similar to Comorian magmas, and

active from over 1.4 to 0.2 Ma. The contrasted morphologies from the Jumelles (polygenic ridges) to Mwezi (monogenic cones and domes), the less evolved composition of magmas in Mwezi together with the more recent radiometric ages, all indicate that volcanism propagated toward the NW along this N135°E structure.

5. The Zélée and Geyser banks are two volcanic seamounts that erupted undersaturated magmas, as did Mohéli and Mayotte islands. Zélée and Geyser were active in the 8–6 Ma interval, coeval with the construction and early emergence of Mayotte. The elongations of Zélée-Geyser from W-E to SW-NE are consistent with the early orientations of Mohéli and Mayotte. All these lines of evidence support that the Zélée and Geyser banks are amongst the oldest and most long-lasting structures of the Comoros Archipelago, together with Mayotte.
6. The N160°E Glorieuses trend of seamounts and atolls has a significantly different major-trace element signature from that of the Comoros Archipelago (including Jumelles-Mwezi and Zélée-Geyser), more enriched in incompatible elements. The Glorieuses trend was constructed from the Turonian to the Maastricthian. The Glorieuses and the Comoros thus represent unrelated magmatic episodes separated by ∼40 Myrs.
7. The Leven Bank, despite being at the junction of the W-E Comoros volcanism and the N160° Glorieuses trend, clearly exhibits a chemical signature akin to the former and distinct from the latter. The volcanism of the Leven Bank was active in the interval 8.5–6 Ma, and coeval with volcanic activity in Mayotte and Zélée-Geyser. The Leven Bank is therefore indisputably one of the easternmost edifices generated by Comorian volcanism.
8. With our new constraints on the ages of the Zélée-Geyser and Leven banks, it is now recognized that Comoros-related volcanism extends eastward to the Cenozoic volcanoes of north Madagascar. The apparent similarities in major and trace element compositions of magmas from the Comoros Archipelago and Cenozoic magmas from northern Madagascar are confirmed by new data. We thus bring conclusive evidence, supporting previous interpretations, that Cenozoic volcanism from north Madagascar to the Comoros belongs to a single, E-W-oriented, 700-km-long and 200-km-wide volcanic chain, active since ≥28 Ma, which we call the MCV chain.
9. Two widespread phases of magmatic renewal occurred along the MCV chain since the Late Miocene, one beginning at 9–8 Ma associated with both structures oriented both NE-SW and NW-SE, and the second one from 2.5 to 0 Ma associated with conspicuous, en-échelon NW-SE-oriented structures. These two magmatic and tectonic phases led to the westward propagation and northward widening of the volcanic chain with time (i.e., toward Grande Comore and the Mwezi volcanic province).
10. Volcano-tectonic reactivation of the MCV chain at 9–8 and 2.5 Ma coincides with modifications of the Somalia plate boundaries (reorganization of the Aden-Owen-Karlsberg triple junction, opening of the Kerimbas Graben), and also coincides with increases in the velocity of the Somalia plate relative to the Lwandle plate. In particular, the systematic en-échelon reorganization of volcano-tectonic structures along the MCV chain is consistent with the kinematic evolution of Somalia relative to Lwandle, from transtension (>3 Ma) to pure dextral strike-slip (≤2.5 Ma) in the northern Mozambique Channel. Our work supports the idea that the MCV chain is indeed the northern segment of the Indian Ocean branch of the EARS and a plate boundary, further pointing to the intimate link between renewed magmatism and the very onset of kinematic reorientations in the Rovuma-Lwandle-Somalia plate system.

Data Availability Statement

Topographic data used to build Figure 1 are publicly available (GEBCO Bathymetric Compilation Group, 2023; Japan Aerospace Exploration Agency, 2021). The complete data set of major and trace elements compositions for samples and geostandards analyzed as part of this research is available at the EarthChem Library (Rusquet et al., 2024).

Acknowledgments

This works is carried out in the framework of the ANR COYOTES (ANR-19-CE31-0018, https://anr.fr/Projet-ANR-19-CE31-0018) project funded by the French ANR (Agence Nationale de la Recherche). This work benefited from three oceanographic expeditions: PAMELA-MOZ01, SISMAORE, and SCRATCH, onboard the R/V L'Atalante, R/V Pourquoi Pas? and R/V Marion Dufresne II, respectively. The oceanographic expedition PAMELA-MOZ01 was co-funded by TOTAL and IFREMER as part of the PAMELA (Passive Margin Exploration Laboratory) scientific project, in collaboration with Université de Bretagne Occidentale, Université Rennes 1, Université Pierre and Marie Curie, CNRS, and IFPEN. The SISMAORE and SCRATCH cruises were mainly funded by the Flotte Océanographique Française (FOF). We are grateful to captains, officers, and crew members of the three cruises for their technical support in recovering high-quality data sets, and the scientific teams for fruitful discussions. Bleuenn Gueguen, Céline Liorzou, and Marie-Laure Rouget are thanked for conducting the major-trace element analyses at PSO. We also thank C. J. Ebinger, T. Rooney, and an anonymous reviewer for their thoughtful comments that greatly improved the manuscript.

References

Argus, D. F., Gordon, R. G., Heflin, M. B., Ma, C., Eanes, R. J., Willis, P., et al. (2010). The angular velocities of the plates and the velocity of Earth's centre from space geodesy. *Geophysical Journal International*, *180*(3), 913–960. https://doi.org/10.1111/j.1365-246X.2009.04463.x

Audru, J.-C., Guennoc, P., Thinon, I., & Abellard, O. (2006). Bathymay: La structure sous-marine de Mayotte révélée par l'imagerie multi-faisceaux. *Comptes Rendus Geoscience*, *338*(16), 1240–1249. https://doi.org/10.1016/j.crte.2006.07.010

Bachèlery, & Hémond (2016). Geochemical and petrological aspects of Karthala volcano. In P. Bachèlery, J.-F. Lénat, A. Di Muro, & L. Michon (Eds.), *Active volcanoes of the Southwest Indian ocean* (pp. 367–384). Springer Berlin Heidelberg. https://doi.org/10.1007/978-3-642-31395-0_23

Bardintzeff, J.-M., Liégeois, J.-P., Bonin, B., Bellon, H., & Rasamimanana, G. (2010). Madagascar volcanic provinces linked to the Gondwana break-up: Geochemical and isotopic evidences for contrasting mantle sources. *Gondwana Research*, *18*(2–3), 295–314. https://doi.org/10.1016/j.gr.2009.11.010

Bazin, S., Royer, J.-Y., Dubost, F., Paquet, F., Loubrieu, B., Lavayssière, A., & the REVOSIMA group. (2022). Initial results from a hydro-acoustic network to monitor submarine lava flows near Mayotte Island. *Comptes Rendus Geoscience*, *354*(S2), 257–273. https://doi.org/10.5802/crgeos.119

Berthod, C., Bachèlery, P., Jorry, S. J., Pitel-Roudaut, M., Ruffet, G., Revillon, S., et al. (2022a). First characterization of the volcanism in the southern Mozambique Channel: Geomorphological and structural analyses. *Marine Geology*, *445*, 106755. https://doi.org/10.1016/j.margeo.2022.106755

Berthod, C., Komorowski, J.-C., Gurioli, L., Médard, E., Bachèlery, P., Besson, P., et al. (2022b). Temporal magmatic evolution of the Fani Maoré submarine eruption 50 km east of Mayotte revealed by in situ sampling and petrological monitoring. *Comptes Rendus Geoscience*, *354*(S2), 195–223. https://doi.org/10.5802/crgeos.155

Berthod, C., Médard, E., Bachèlery, P., Gurioli, L., Di Muro, A., Peltier, A., et al. (2021b). The 2018-ongoing Mayotte submarine eruption: Magma migration imaged by petrological monitoring. *Earth and Planetary Science Letters*, *571*, 117085. https://doi.org/10.1016/j.epsl.2021.117085

Berthod, C., Médard, E., Di Muro, A., Hassen Ali, T., Gurioli, L., Chauvel, C., et al. (2021c). Mantle xenolith-bearing phonolites and basanites feed the active volcanic ridge of Mayotte (Comoros Archipelago, SW Indian Ocean). *Contributions to Mineralogy and Petrology*, *176*(10), 75. https://doi.org/10.1007/s00410-021-01833-1

Berthod, C., Zaragosi, S., & Famin, V. (2021a). *SCRATCH cruise, R/V Marion Dufresne*. https://doi.org/10.17600/18002274

Bertil, D., Mercury, N., Doubre, C., Lemoine, A., & Van der Woerd, J. (2021). The unexpected Mayotte 2018–2020 seismic sequence: A reappraisal of the regional seismicity of the Comoros. *Comptes Rendus Geoscience*, *353*(S1), 211–235. https://doi.org/10.5802/crgeos.79

Bordenca, C. V., Faccini, B., Caracausi, A., Coltorti, M., Di Muro, A., Pik, R., et al. (2023). The nature of the mantle beneath La Grille volcano (Grande Comore Island, western Indian Ocean) as revealed by mineral chemistry, noble gas geochemistry, CO_2 abundance and radiogenic isotopes of ultramafic mantle xenoliths. *Lithos*, *462–463*, 107406. https://doi.org/10.1016/j.lithos.2023.107406

Boyce, A., Kounoudis, R., Bastow, I. D., Cottaar, S., Ebinger, C. J., & Ogden, C. S. (2023). Mantle wavespeed and discontinuity structure below East Africa: Implications for Cenozoic hotspot tectonism and the development of the Turkana depression. *Geochemistry, Geophysics, Geosystems*, *24*(8), e2022GC010775. https://doi.org/10.1029/2022GC010775

Buchwaldt, R. (2006). *Geology of the neoproterozoic and cenozoic rocks of northnorth Madagascar*. Washington University.

Cesca, S., Letort, J., Razafindrakoto, H. N. T., Heimann, S., Rivalta, E., Isken, M. P., et al. (2020). Drainage of a deep magma reservoir near Mayotte inferred from seismicity and deformation. *Nature Geoscience*, *13*(1), 87–93. https://doi.org/10.1038/s41561-019-0505-5

Class, C., Goldstein, S., Stute, M., Kurz, M., & Schlosser, P. (2005). Grand Comore island: A well-constrained "low 3He/4He" mantle plume. *Earth and Planetary Science Letters*, *233*(3–4), 391–409. https://doi.org/10.1016/j.epsl.2005.02.029

Class, C., & Goldstein, S. L. (1997). Plume-lithosphere interactions in the ocean basins: Constraints from the source mineralogy. *Earth and Planetary Science Letters*, *150*(3–4), 245–260. https://doi.org/10.1016/S0012-821X(97)00089-7

Class, C., Goldstein, S. L., Altherr, R., & Bachèlery, P. (1998). The process of plume–lithosphere interactions in the ocean basins—The case of Grande Comore. *Journal of Petrology*, *39*(5), 881–903. https://doi.org/10.1093/petroj/39.5.881

Class, C., Goldstein, S. L., & Shirey, S. B. (2009). Osmium isotopes in Grande Comore lavas: A new extreme among a spectrum of EM-type mantle endmembers. *Earth and Planetary Science Letters*, *284*(1), 219–227. https://doi.org/10.1016/j.epsl.2009.04.031

Claude-Ivanaj, C., Bourdon, B., & Allègre, C. J. (1998). Ra–Th–Sr isotope systematics in Grande Comore island: A case study of plume–lithosphere interaction. *Earth and Planetary Science Letters*, *164*(1), 99–117. https://doi.org/10.1016/S0012-821X(98)00195-2

Cotten, J., Le Dez, A., Bau, M., Caroff, M., Maury, R. C., Dulski, P., et al. (1995). Origin of anomalous rare-earth element and yttrium enrichments in subaerially exposed basalts: Evidence from French Polynesia. *Chemical Geology*, *119*(1–4), 115–138. https://doi.org/10.1016/0009-2541(94)00102-E

Courgeon, S., Bachèlery, P., Jouet, G., Jorry, S. J., Bou, E., BouDagher-Fadel, M. K., et al. (2018). The offshore east African rift system: New insights from the Sakalaves seamounts (Davie Ridge, SW Indian Ocean). *Terra Nova*, *30*(5), 380–388. https://doi.org/10.1111/ter.12353

Courgeon, S., Jorry, S. J., Camoin, G. F., BouDagher-Fadel, M. K., Jouet, G., Révillon, S., et al. (2016). Growth and demise of Cenozoic isolated carbonate platforms: New insights from the Mozambique Channel seamounts (SW Indian Ocean). *Marine Geology*, *380*, 90–105. https://doi.org/10.1016/j.margeo.2016.07.006

Cucciniello, C., Grifa, C., de'Gennaro, R., Franciosi, L., Rocco, I., Morra, V., & Melluso, L. (2022). Alkaline rocks of the Bobaomby volcanic field point to a petrogenetic link between Comoros and northern Madagascar lithosphere. *International Journal of Earth Sciences*, *112*(2), 707–723. https://doi.org/10.1007/s00531-022-02251-9

Cucciniello, C., Melluso, L., Morra, V., Storey, M., Rocco, I., Franciosi, L., et al. (2011). New ^{40}Ar-^{39}Ar ages and petrogenesis of the Massif d'Ambre volcano, northern Madagascar. In L. Beccaluva, G. Bianchini, & M. Wilson (Eds.), *Volcanism and evolution of the African lithosphere* (Vol. 478, pp. 257–281). Geological Society of America. https://doi.org/10.1130/2011.2478(14

Cucciniello, C., Tucker, R. D., Jourdan, F., Melluso, L., & Morra, V. (2016). The age and petrogenesis of alkaline magmatism in the Ampasindava Peninsula and Nosy Be Archipelago, northern Madagascar. *Mineralogy and Petrology*, *110*(2–3), 309–331. https://doi.org/10.1007/s00710-015-0387-1

Daniel, J., Dupont, J., & Jouannic, C. (1972). Relations Madagascar-archipel des Comores (Nord-Est du canal du Mozambique): Sur la nature volcanique du Banc du Leven. *Comptes Rendus de l'Académie Des Sciences. Série D: Science and Nature*, *274*, 1784–1787.

Debeuf, D. (2004). *Étude de l'évolution volcano-structurale et magmatique de Mayotte, Archipel des Comores, océan Indien: Approches structurale, pétrographique, géochimique et géochronologique* (p. 243). Université de la Réunion.

DeMets, C., Merkouriev, S., & Sauter, D. (2015). High-resolution estimates of Southwest Indian Ridge plate motions, 20 Ma to present. *Geophysical Journal International*, *203*(3), 1495–1527. https://doi.org/10.1093/gji/ggv366

DeMets, C., Merkouriev, S., & Sauter, D. (2021). High resolution reconstructions of the Southwest Indian Ridge, 52 Ma to present: Implications for the breakup and absolute motion of the Africa plate. *Geophysical Journal International*, *226*(3), 1461–1497. https://doi.org/10.1093/gji/ggab107

Deniel, C. (1998). Geochemical and isotopic (Sr, Nd, Pb) evidence for plume–lithosphere interactions in the genesis of Grande Comore magmas (Indian Ocean). *Chemical Geology*, *144*(3–4), 281–303. https://doi.org/10.1016/S0009-2541(97)00139-3

Desgrolard, F. (1996). *Pétrologie des laves d'un volcan intraplaque océanique: Le Karthala, île de la Grande-Comore (R.F.I. des Comores)* (p. 176). Université Joseph-Fourier - Grenoble I.

Deville, E., Marsset, T., Courgeon, S., Jatiault, R., Ponte, J.-P., Thereau, E., et al. (2018). Active fault system across the oceanic lithosphere of the Mozambique Channel: Implications for the Nubia–Somalia southern plate boundary. *Earth and Planetary Science Letters*, *502*, 210–220. https://doi.org/10.1016/j.epsl.2018.08.052

Dodson, M. H. (1973). Closure temperature in cooling geochronological and petrological systems. *Contributions to Mineralogy and Petrology*, *40*(3), 259–274. https://doi.org/10.1007/BF00373790

Dongmo Wamba, M., Montagner, J.-P., & Romanovicz, B. (2023). Imaging deep-mantle plumbing beneath La Réunion and Comores hot spots: Vertical plume conduits and horizontal ponding zones. *Science Advances*, *9*(4), eade3723. https://doi.org/10.1126/sciadv.ade3723

Ebinger, C. J., Yemane, T., Harding, D. J., Tesfaye, S., Kelley, S., & Rex, D. C. (2000). Rift deflection, migration, and propagation: Linkage of the Ethiopian and Eastern rifts, Africa. *Geological Society of America Bulletin*, *112*(2), 163–176. https://doi.org/10.1130/0016-7606(2000)112%3C163:RDMAPL%3E2.0.CO;2

Emerick, C. M., & Duncan, R. A. (1982). Age progressive volcanism in the Comores Archipelago, western Indian Ocean and implications for Somali plate tectonics. *Earth and Planetary Science Letters*, *60*(3), 415–428. https://doi.org/10.1016/0012-821X(82)90077-2

Emerick, C. M., & Duncan, R. A. (1983). Errata. *Earth and Planetary Science Letters*, *62*(3), 439. https://doi.org/10.1016/0012-821X(83)90014-6

Estrade, G., Béziat, D., Salvi, S., Tiepolo, M., Paquette, J.-L., & Rakotovao, S. (2014). Unusual evolution of silica-under- and -oversaturated alkaline rocks in the Cenozoic Ambohimirahavavy Complex (Madagascar): Mineralogical and geochemical evidence. *Lithos*, *206–207*, 361–383. https://doi.org/10.1016/j.lithos.2014.08.008

Famin, V., Michon, L., & Bourhane, A. (2020). The Comoros archipelago: A right-lateral transform boundary between the Somalia and Lwandle plates. *Tectonophysics*, *789*, 228539. https://doi.org/10.1016/j.tecto.2020.228539

Farley, K. A. (2002). (U-Th)/He dating: Techniques, calibrations, and applications. *Reviews in Mineralogy and Geochemistry*, *47*(1), 819–844. https://doi.org/10.2138/rmg.2002.47.18

Farley, K. A., Wolf, R. A., & Silver, L. T. (1996). The effects of long alpha-stopping distances on (U-Th)/He ages. *Geochimica et Cosmochimica Acta*, *60*(21), 4223–4229. https://doi.org/10.1016/S0016-7037(96)00193-7

Feuillet, N., Jorry, S., Crawford, W. C., Deplus, C., Thinon, I., Jacques, E., et al. (2021). Birth of a large volcanic edifice offshore Mayotte via lithosphere-scale dyke intrusion. *Nature Geoscience*, *14*(10), 787–795. https://doi.org/10.1038/s41561-021-00809-x

Flower, M. F. J. (1971). Rare earth element distribution in lavas and ultramafic xenoliths from the Comores Archipelago, Western Indian Ocean. *Contributions to Mineralogy and Petrology*, *31*(4), 335–346. https://doi.org/10.1007/BF00371153

Flower, M. F. J. (1973). Evolution of basaltic and differentiated lavas from Anjouan, Comores archipelago. *Contributions to Mineralogy and Petrology*, *38*(3), 237–260. https://doi.org/10.1007/BF00374768

Franke, D., Jokat, W., Ladage, S., Stollhofen, H., Klimke, J., Lutz, R., et al. (2015). The offshore East African Rift System: Structural framework at the toe of a juvenile rift. *Tectonics*, *34*(10), 2086–2104. https://doi.org/10.1002/2015TC003922

GEBCO Bathymetric Compilation Group. (2023). The GEBCO_2023 Grid—A continuous terrain model of the global oceans and land. (Version 1) [documents, network common data form]. *NERC EDS British Oceanographic Data Centre NOC*. https://doi.org/10.5285/f98b053b-0cbc-6c23-e053-6c86abc0af7b

Graham, S. E., Loveless, J. P., & Meade, B. J. (2018). Global Plate motions and earthquake cycle effects. *Geochemistry, Geophysics, Geosystems*, *19*(7), 2032–2048. https://doi.org/10.1029/2017GC007391

Guenthner, W. R., Reiners, P. W., Ketcham, R. A., Nasdala, L., & Giester, G. (2013). Helium diffusion in natural zircon: Radiation damage, anisotropy, and the interpretation of zircon (U-Th)/He thermochronology. *American Journal of Science*, *313*(3), 145–198. https://doi.org/10.2475/03.2013.01

Hajash, A., & Armstrong, R. L. (1972). Paleomagnetic and radiometric evidence for the age of the Comores Islands, west central Indian Ocean. *Earth and Planetary Science Letters*, *16*(2), 231–236. https://doi.org/10.1016/0012-821X(72)90195-1

Iacopini, D., Tavani, S., Pentagallo, S., Maselli, V., Dottore Stagna, M., Ebinger, C., et al. (2022). Architecture, structural and tectonic significance of the Seagap fault (offshore Tanzania) in the framework of the East African Rift. *Basin Research*, *35*(1), 387–412. https://doi.org/10.1111/bre.12716

International Union of Geological Sciences. (2005). In R. W. LeMaitre (Ed.), *Igneous rocks: A classification and glossary of terms: Recommendation of the international union of geological Sciences, subcommission on the systematics of igneous rocks* (Vol. 2). Cambridge Univ. Press.

Japan Aerospace Exploration Agency. (2021). ALOS world 3D - 30m DEM (version 3.2) [dataset]. *OpenTopography*. https://doi.org/10.5069/G94M92HB

Jochum, K. P., Weis, U., Schwager, B., Stoll, B., Wilson, S. A., Haug, G. H., et al. (2016). Reference values following ISO guidelines for frequently requested rock reference materials. *Geostandards and Geoanalytical Research*, *40*(3), 333–350. https://doi.org/10.1111/j.1751-908X.2015.00392.x

King, R., Floyd, M., Reilinger, R., & Bendick, R. (2019). GPS velocity field (MIT 2019.0) for the East African Rift System generated by King et al. (Version 1) [Text/plain]. *Interdisciplinary Earth Data Alliance (IEDA)*. https://doi.org/10.1594/IEDA/324785

Klimke, J., Franke, D., Gaedicke, C., Schreckenberger, B., Schnabel, M., Stollhofen, H., et al. (2016). How to identify oceanic crust-Evidence for a complex break-up in the Mozambique Channel, off East Africa. *Tectonophysics*, *693*, 436–452. https://doi.org/10.1016/j.tecto.2015.10.012

Kreemer, C., Blewitt, G., & Klein, E. C. (2014). A geodetic plate motion and global strain rate model. *Geochemistry, Geophysics, Geosystems*, *15*(10), 3849–3889. https://doi.org/10.1002/2014GC005407

Lacombe, T., Gurioli, L., Di Muro, A., Médard, E., Berthod, C., Bachèlery, P., et al. (2024). Late quaternary explosive phonolitic volcanism of Petite-Terre (Mayotte, western Indian ocean). *Bulletin of Volcanology*, *86*(2), 11. https://doi.org/10.1007/s00445-023-01697-2

Le Bas, M. J., Le Maitre, R. W., Streckeisen, A., & Zanettin, B., & IUGS Subcommission on the Systematics of Igneous Rocks. (1986). A chemical classification of volcanic rocks based on the total alkali-silica diagram. *Journal of Petrology*, *27*(3), 745–750. https://doi.org/10.1093/petrology/27.3.745

Lemoine, A., Briole, P., Bertil, D., Roullé, A., Foumelis, M., Thinon, I., et al. (2020). The 2018–2019 seismo-volcanic crisis east of Mayotte, Comoros islands: Seismicity and ground deformation markers of an exceptional submarine eruption. *Geophysical Journal International*, *223*(1), 22–44. https://doi.org/10.1093/gji/ggaa273

Leroux, E., Counts, J. W., Jorry, S. J., Jouet, G., Révillon, S., BouDagher-Fadel, M. K., et al. (2020). Evolution of the Glorieuses seamount in the SW Indian Ocean and surrounding deep Somali basin since the cretaceous. *Marine Geology*, *427*, 106202. https://doi.org/10.1016/j.margeo.2020.106202

Lyubetskaya, T., & Korenaga, J. (2007). Chemical composition of Earth's primitive mantle and its variance: 1. Method and results. *Journal of Geophysical Research*, *112*(B3), B03211. https://doi.org/10.1029/2005JB004223

Mana, S., Furman, T., Turrin, B. D., Feigenson, M. D., & Swisher, C. C. (2015). Magmatic activity across the East African north Tanzanian divergence zone. *Journal of the Geological Society*, *172*(3), 368–389. https://doi.org/10.1144/jgs2014-072

Martin, K. A. (2023). Opposite microplate rotations on the East African Rift: Similarity to double saloon door tectonics. *Journal of African Earth Sciences*, *198*, 104803. https://doi.org/10.1016/j.jafrearsci.2022.104803

Mascle, J., Mougenot, D., Blarez, E., Marinho, M., & Virlogeux, P. (1987). African transform continental margins: Examples from Guinea, the ivory coast and Mozambique. *Geological Journal*, *22*(S2), 537–561. https://doi.org/10.1002/gj.3350220632

Masquelet, C., Leroy, S., Delescluse, M., Chamot-Rooke, N., Thinon, I., Lemoine, A., et al. (2022). The East-Mayotte new volcano in the Comoros archipelago: Structure and timing of magmatic phases inferred from seismic reflection data. *Comptes Rendus Geoscience*, *354*(S2), 65–79. https://doi.org/10.5802/crgeos.154

Masquelet, C., Watremez, L., Leroy, S., Sauter, D., Delescluse, M., Chamot-Rooke, N., et al. (2024). Intra-oceanic emplacement of the Comoros Archipelago through inherited fracture zones. *Tectonophysics*, *882*, 230348. https://doi.org/10.1016/j.tecto.2024.230348

McDougall, I., & Harrison, T. M. (1999). *Geochronology and thermochronology by the 40Ar/39Ar method* (p. 242). Oxford University Press.

Melluso, L., & Morra, V. (2000). Petrogenesis of late Cenozoic mafic alkaline rocks of the Nosy Be archipelago (northern Madagascar): Relationships with the Comorean magmatism. *Journal of Volcanology and Geothermal Research*, *96*(1–2), 129–142. https://doi.org/10.1016/S0377-0273(99)00139-0

Melluso, L., Morra, V., Riziky, H., Veloson, J., Lustrino, M., Del Gatto, L., & Modeste, V. (2007). Petrogenesis of a basanite–tephrite–phonolite volcanic suite in the Bobaomby (Cap d'Ambre) peninsula, northern Madagascar. *Journal of African Earth Sciences*, *49*(1–2), 29–42. https://doi.org/10.1016/j.jafrearsci.2007.06.002

Michon, L. (2016). The volcanism of the Comoros archipelago integrated at a regional scale. In P. Bachelery, J.-F. Lenat, A. Di Muro, & L. Michon (Eds.), *Active volcanoes of the Southwest Indian ocean* (pp. 333–344). Springer Berlin Heidelberg. https://doi.org/10.1007/978-3-642-31395-0_21

Michon, L., Famin, V., & Quidelleur, X. (2022). Evolution of the East African Rift System from trap-scale to plate-scale rifting. *Earth-Science Reviews*, *231*, 104089. https://doi.org/10.1016/j.earscirev.2022.104089

Nougier, J., Cantagrel, J. M., & Karche, J. P. (1986). The Comores archipelago in the western Indian Ocean: Volcanology, geochronology and geodynamic setting. *Journal of African Earth Sciences*, *5*(2), 135–145. https://doi.org/10.1016/0899-5362(86)90003-5

Oliva, S. J., Ebinger, C. J., Rivalta, E., Williams, C. A., Wauthier, C., & Currie, C. A. (2022). State of stress and stress rotations: Quantifying the role of surface topography and subsurface density contrasts in magmatic rift zones (Eastern Rift, Africa). *Earth and Planetary Science Letters*, *584*, 117478. https://doi.org/10.1016/j.epsl.2022.117478

Olu, K. (2014). PAMELA-MOZ01 cruise. *R/V L'Atalante*. https://doi.org/10.17600/14001000

Pelleter, A.-A., Caroff, M., Cordier, C., Bachelery, P., Nehlig, P., Debeuf, D., & Arnaud, N. (2014). Melilite-bearing lavas in Mayotte (France): An insight into the mantle source below the Comores. *Lithos*, *208–209*, 281–297. https://doi.org/10.1016/j.lithos.2014.09.012

Phethean, J. J. J., Kalnins, L. M., Van Hunen, J., Biffi, P. G., Davies, R. J., & McCaffrey, K. J. W. (2016). Madagascar's escape from Africa: A high-resolution plate reconstruction for the western Somali basin and implications for supercontinent dispersal. *Geochemistry, Geophysics, Geosystems*, *17*(12), 5036–5055. https://doi.org/10.1002/2016GC006624

Quidelleur, X., Michon, L., Famin, V., Geffray, M.-C., Danišík, M., Gardiner, N., et al. (2022). Holocene volcanic activity in Anjouan Island (Comoros Archipelago) revealed by new Cassignol-Gillot groundmass K–Ar and 14C ages. *Quaternary Geochronology*, *67*, 101236. https://doi.org/10.1016/j.quageo.2021.101236

Roche, V., & Ringenbach, J.-C. (2022). The Davie fracture zone: A recorder of continents drifts and kinematic changes. *Tectonophysics*, *823*, 229188. https://doi.org/10.1016/j.tecto.2021.229188

Rodriguez, M., Fournier, M., Chamot-Rooke, N., Huchon, P., & Delescluse, M. (2018). The geological evolution of the Aden-Owen-Carlsberg triple junction (NW Indian ocean) since the late Miocene. *Tectonics*, *37*(5), 1552–1575. https://doi.org/10.1029/2017TC004687

Roig, J. Y., Tucker, R. D., Peters, S. G., Delor, C., & Théveniaut, H. (2012). Carte géologique de la République de Madagascar à 1/1 000 000. (Ministère des Mines, PGRM) [Map].

Rolandone, F., Poort, J., Masquelet, C., Leroy, S., Thinon, I., Lemoine, A., & Paquet, F. (2022). Heat flow measurements in the northern Mozambique channel. *Comptes Rendus Geoscience*, *354*(S2), 35–46. https://doi.org/10.5802/crgeos.130

Rooney, T. O. (2020). The Cenozoic magmatism of East Africa: Part III–Rifting of the craton. *Lithos*, *360–361*, 105390. https://doi.org/10.1016/j.lithos.2020.105390

Rusquet, A., Famin, V., Michon, L., Quidelleur, X., Nauret, F., Danišík, M., et al. (2024). Major and trace elements analyses of volcanic rocks from the Comoros and Glorieuses archipelagos (western Indian Ocean) (version 1.0) [Dataset]. *Interdisciplinary Earth Data Alliance (IEDA)*. https://doi.org/10.60520/IEDA/113462

Rusquet, A., Famin, V., Quidelleur, X., Michon, L., Nauret, F., Danišík, M., et al. (2023). Pliocene-to-Holocene volcano-tectonic activity on Mohéli Island (Comoros Archipelago) constrained by new K-Ar ages. *Journal of Volcanology and Geothermal Research*, *442*, 107896. https://doi.org/10.1016/j.jvolgeores.2023.107896

Saria, E., Calais, E., Stamps, D. S., Delvaux, D., & Hartnady, C. J. H. (2014). Present-day kinematics of the East African Rift. *Journal of Geophysical Research: Solid Earth*, *119*(4), 3584–3600. https://doi.org/10.1002/2013JB010901

Späth, A., Roex, A. P. L., & Duncan, R. A. (1996). The geochemistry of lavas from the Gomores archipelago, western Indian ocean: Petrogenesis and mantle source region characteristics. *Journal of Petrology*, *37*(4), 961–991. https://doi.org/10.1093/petrology/37.4.961

Stamps, D. S., Saria, E., & Kreemer, C. (2018). A geodetic strain rate model for the East African Rift System. *Scientific Reports*, *8*(1), 732. https://doi.org/10.1038/s41598-017-19097-w

Strong, D. F. (1972a). The petrology of the lavas of Grande Comore. *Journal of Petrology*, *13*(2), 181–218. https://doi.org/10.1093/petrology/13.2.181

Strong, D. F. (1972b). Petrology of the island of Moheli, western Indian ocean. *Geological Society of America Bulletin*, *83*(2), 389. https://doi.org/10.1130/0016-7606(1972)83[389:POTIOM]2.0.CO;2

Thinon, I., Lemoine, A., Leroy, S., Paquet, F., Berthod, C., Zaragosi, S., et al. (2022). Volcanism and tectonics unveiled in the Comoros archipelago between Africa and Madagascar. *Comptes Rendus Geoscience*, *354*(S2), 7–34. https://doi.org/10.5802/crgeos.159

Thinon, I., Leroy, S., & Lemoine, A. (2021). SISMAORE cruise, R/V Pourquoi pas? https://doi.org/10.17600/18001331

Thivet, S., Carlier, J., Gurioli, L., Di Muro, A., Besson, P., Smietana, M., et al. (2022). Magmatic and phreatomagmatic contributions on the ash-dominated basaltic eruptions: Insights from the April and November–December 2005 paroxysmal events at Karthala volcano, Comoros. *Journal of Volcanology and Geothermal Research*, *424*, 107500. https://doi.org/10.1016/j.jvolgeores.2022.107500

Thompson, R. N., & Flower, M. F. J. (1971). One-atmosphere melting and crystallization relations of lavas from Anjouan, Comores archipelago, western Indian ocean. *Earth and Planetary Science Letters*, *12*(1), 97–107. https://doi.org/10.1016/0012-821X(71)90060-4

Tucker, R. D., Conrad, J., Key, R. M., Pitfield, P. E. J., Randriamananjara, T., Taylor, C. D., et al. (2008). 40Ar/39Ar geochronology of Mesozoic and younger igneous rocks, Madagascar Revision of the geologic and mineral cartography of the north, central and east-central zones of

Madagascar; explanatory note to the Republic of Madagascar, Ministry of Energy and Mines (MEM/SG/DG/UCP/PGRM). *Geologic and Commission Report*, 385–435.

Tzevahirtzian, A., Zaragosi, S., Bachèlery, P., Biscara, L., & Marchès, E. (2021). Submarine morphology of the Comoros volcanic archipelago. *Marine Geology*, *432*, 106383. https://doi.org/10.1016/j.margeo.2020.106383

Wang, S., Yu, H., Zhang, Q., & Zhao, Y. (2018). Absolute plate motions relative to deep mantle plumes. *Earth and Planetary Science Letters*, *490*, 88–99. https://doi.org/10.1016/j.epsl.2018.03.021

York, D. (1968). Least squares fitting of a straight line with correlated errors. *Earth and Planetary Science Letters*, *5*, 320–324. https://doi.org/10.1016/S0012-821X(68)80059-7

York, D., Evensen, N. M., Martínez, M. L., & De Basabe Delgado, J. (2004). Unified equations for the slope, intercept, and standard errors of the best straight line. *American Journal of Physics*, *72*(3), 367–375. https://doi.org/10.1119/1.1632486

Zinke, J., Reijmer, J. J. G., & Thomassin, B. A. (2003). Systems tracts sedimentology in the lagoon of Mayotte associated with the Holocene transgression. *Sedimentary Geology*, *160*(1–3), 57–79. https://doi.org/10.1016/S0037-0738(02)00336-6

References From the Supporting Information

Bachèlery, P., & Coudray, J. (1993). *Carte volcano-tectonique de la Grande Comore (Ngazidja) et notice explicative* (French Embassy in Moroni, Comores, and University of La Réunion, St. Denis de La Réunion).

Cassignol, C., & Gillot, P.-Y. (1982). Range and effectiveness of unspiked potassium-argon dating: Experimental groundwork and applications. In G. S. Odin (Ed.), *Numerical dating in stratigraphy* (pp. 159–179). Wiley.

Cheilletz, A., Ruffet, G., Marignac, C., Kolli, O., Gasquet, D., Féraud, G., & Bouillin, J. P. (1999). $^{40}Ar/^{39}Ar$ dating of shear zones in the Variscan basement of greater Kabylia (Algeria). Evidence of an Eo-Alpine event at 128 Ma (Hauterivian–Barremian boundary): Geodynamic consequences. *Tectonophysics*, *306*(1), 97–116. https://doi.org/10.1016/S0040-1951(99)00047-5

Danišík, M., Kuhlemann, J., Dunkl, I., Evans, N. J., Székely, B., & Frisch, W. (2012a). Survival of ancient landforms in a collisional setting as revealed by combined fission track and (U-Th)/He thermochronometry: A case study from Corsica (France). *The Journal of Geology*, *120*(2), 155–173. https://doi.org/10.1086/663873

Danišík, M., Štěpančíková, P., & Evans, N. J. (2012b). Constraining long-term denudation and faulting history in intraplate regions by multi-system thermochronology: An example of the Sudetic Marginal Fault (Bohemian Massif, central Europe). *Tectonics*, *31*(2), TC2003. https://doi.org/10.1029/2011TC003012

Duncan, R. A., & Hogan, L. G. (1994). Radiometric dating of young MORB using the ^{40} Ar- ^{39} Ar incremental heating method. *Geophysical Research Letters*, *21*(18), 1927–1930. https://doi.org/10.1029/94GL01375

Evans, N. J., Byrne, J. P., Keegan, J. T., & Dotter, L. E. (2005). Determination of uranium and thorium in zircon, apatite, and fluorite: Application to laser (U-Th)/He thermochronology. *Journal of Analytical Chemistry*, *60*(12), 1159–1165. https://doi.org/10.1007/s10809-005-0260-1

Fuhrmann, U., Lippolt, H. J., & Hess, J. C. (1987). Examination of some proposed K-Ar standards: Analyses and conventional K-Ar data. *Chemical Geology: Isotope Geoscience section*, *66*(1–2), 41–51. https://doi.org/10.1016/0168-9622(87)90027-3

Germa, A., Quidelleur, X., Labanieh, S., Lahitte, P., & Chauvel, C. (2010). The eruptive history of Morne Jacob volcano (Martinique Island, French West Indies): Geochronology, geomorphology and geochemistry of the earliest volcanism in the recent Lesser Antilles arc. *Journal of Volcanology and Geothermal Research*, *198*(3–4), 297–310. https://doi.org/10.1016/j.jvolgeores.2010.09.013

Gillot, P.-Y., Cornette, Y., Max, N., & Floris, B. (1992). Two reference materials, trachytes MDO-G and ISH-G, for argon dating (K-Ar and $^{40}Ar/^{39}Ar$) of Pleistocene and Holocene rocks. *Geostandards and Geoanalytical Research*, *16*(1), 55–60. https://doi.org/10.1111/j.1751-908X.1992.tb00487.x

Gillot, P.-Y., Hildenbrand, A., Lefèvre, J.-C., & Albore-Livadie, C. (2006). The K/Ar dating method: Principle, analytical techniques, and application to Holocene volcanic eruptions in southern Italy. *Acta Vulcanologica: Journal of the National Volcanic Group of Italy*, *1/2*. https://doi.org/10.1400/93820

Henri, M., Quidelleur, X., Le Friant, A., Komorowski, J.-C., Escartín, J., Deplus, C., & Mevel, C. (2022). K-Ar Geochronology and geochemistry of underwater lava samples from the Subsaintes cruise offshore Les Saintes (Guadeloupe): Insights for the Lesser Antilles arc magmatism. *Marine Geology*, *450*, 106862. https://doi.org/10.1016/j.margeo.2022.106862

Hess, J. C., & Lippolt, H. J. (1994). Compilation of K/Ar measurements on HD-B1 standard biotite; 1994 status report. In *Phanerozoic time scale*. Bulletin de Liaison et d'information, IUGS Subcommission. *Geochronology*, *12*, 19–23.

Lee, J.-Y., Marti, K., Severinghaus, J. P., Kawamura, K., Yoo, H.-S., Lee, J. B., & Kim, J. S. (2006). A redetermination of the isotopic abundances of atmospheric Ar. *Geochimica et Cosmochimica Acta*, *70*(17), 4507–4512. https://doi.org/10.1016/j.gca.2006.06.1563

Mark, D. F., Stuart, F. M., & De Podesta, M. (2011). New high-precision measurements of the isotopic composition of atmospheric argon. *Geochimica et Cosmochimica Acta*, *75*(23), 7494–7501. https://doi.org/10.1016/j.gca.2011.09.042

McDowell, F. W., McIntosh, W. C., & Farley, K. A. (2005). A precise $^{40}Ar–^{39}Ar$ reference age for the Durango apatite (U–Th)/He and fission-track dating standard. *Chemical Geology*, *214*(3–4), 249–263. https://doi.org/10.1016/j.chemgeo.2004.10.002

Raczek, I., Stoll, B., Hofmann, A. W., & Peter Jochum, K. (2001). High-precision trace element data for the USGS reference materials BCR-1, BCR-2, BHVO-1, BHVO-2, AGV-1, AGV-2, DTS-1, DTS-2, GSP-1 and GSP-2 by ID-TIMS and MIC-SSMS. *Geostandards and Geoanalytical Research*, *25*(1), 77–86. https://doi.org/10.1111/j.1751-908X.2001.tb00789.x

Reiners, P. W. (2005). Zircon (U-Th)/He thermochronometry. *Reviews in Mineralogy and Geochemistry*, *58*(1), 151–179. https://doi.org/10.2138/rmg.2005.58.6

Renne, P. R., Mundil, R., Balco, G., Min, K., & Ludwig, K. R. (2010). Joint determination of ^{40}K decay constants and $^{40}Ar^*/^{40}K$ for the Fish Canyon sanidine standard, and improved accuracy for $^{40}Ar/^{39}Ar$ geochronology. *Geochimica et Cosmochimica Acta*, *74*(18), 5349–5367. https://doi.org/10.1016/j.gca.2010.06.017

Renne, P. R., Balco, G., Ludwig, K. R., Mundil, R., & Min, K. (2011). Response to the comment by W.H. Schwarz et al. On "Joint determination of ^{40}K decay constants and $^{40}Ar^*/^{40}K$ for the Fish Canyon sanidine standard, and improved accuracy for $^{40}Ar/^{39}Ar$ geochronology" by P.R. Renne et al. (2010). *Geochimica et Cosmochimica Acta*, *75*(17), 5097–5100. https://doi.org/10.1016/j.gca.2011.06.021

Ruffet, G., Féraud, G., & Amouric, M. (1991). Comparison of ^{40}Ar-^{39}Ar conventional and laser dating of biotites from the North Trégor Batholith. *Geochimica et Cosmochimica Acta*, *55*(6), 1675–1688. https://doi.org/10.1016/0016-7037(91)90138-U

Ruffet, G., Féraud, G., Balèvre, M., & Kiénast, J.-R. (1995). Plateau ages and excess argon in phengites: An $^{40}Ar/^{39}Ar$ laser probe study of Alpine micas (Sesia Zone, Western Alps, northern Italy). *Chemical Geology*, *121*(1–4), 327–343. https://doi.org/10.1016/0009-2541(94)00132-R

Ruffet, G., Gruau, G., Ballèvre, M., Féraud, G., & Philippot, P. (1997). Rb/Sr and $^{40}Ar/^{39}Ar$ laser probe dating of high-pressure phengites from the Sesia zone (Western Alps): Underscoring of excess argon and new age constraints on the high-pressure metamorphism. *Chemical Geology*, *141*(1–2), 1–18. https://doi.org/10.1016/S0009-2541(97)00052-1

Schaen, A. J., Jicha, B. R., Hodges, K. V., Vermeesch, P., Stelten, M. E., Mercer, C. M., et al. (2020). Interpreting and reporting $^{40}Ar/^{39}Ar$ geochronologic data. *Geological Society of America Bulletin*, *133*(3–4), 461–487. https://doi.org/10.1130/B35560.1

Schwarz, W. H., & Trieloff, M. (2007). Intercalibration of ^{40}Ar–^{39}Ar age standards NL-25, HB3gr hornblende, GA1550, SB-3, HD-B1 biotite and BMus/2 muscovite. *Chemical Geology*, *242*(1–2), 218–231. https://doi.org/10.1016/j.chemgeo.2007.03.016

Steiger, R. H., & Jäger, E. (1977). Subcommission on geochronology: Convention on the use of decay constants in geo- and cosmochronology. *Earth and Planetary Science Letters*, *36*(3), 359–362. https://doi.org/10.1016/0012-821X(77)90060-7

Bachèlery, P., Morin, J., Villeneuve, N., Soulé, H., Nassor, H., & Ali, A. R. (2016). Structure and eruptive history of Karthala volcano. In P. Bachelery, J.-F. Lenat, A. Di Muro, & L. Michon (Eds.), *Active volcanoes of the Southwest Indian ocean* (pp. 345–366). Springer Berlin Heidelberg. https://doi.org/10.1007/978-3-642-31395-0_22